Enhanced electromagnetic interference shielding effectiveness of polypropylene/hybrid metallic fillers composite materials by coalescence-driven guided electrical percolation

H. Lecocq, G. Sudre, P. Alcouffe, O. Lhost, P. Cassagnau, A. Serghei

Enhanced electromagnetic interference shielding of polypropylene/hybrid metallic fillers composite materials by coalescence-driven guided electrical percolation

H. Lecocq[1], G. Sudre[1], P. Alcouffe[1], O. Lhost[2], P. Cassagnau[1], A. Serghei[1]

[1]*Université Claude Bernard Lyon 1, IMP, CNRS, UMR 5223, 69622 Villeurbanne, FRANCE*

[2]*TOTAL Research and Technology Feluy, C 7181, Feluy, BELGIUM*

Abstract: The electromagnetic interference shielding properties of polypropylene-based composite materials filled with two different types of metallic fillers (hybrid Ag-coated glass microfibers and Tin microparticles) have been investigated between 0.1 MHz and 18 GHz. Two different experimental techniques were employed: coaxial cell method and waveguide method. We show that a substantial enhancement in the shielding effectiveness by more than 60 dB can be obtained by a phenomenon of guided electrical percolation. This phenomenon takes places due to a drastic change in the composite morphology from a homogeneous to a highly heterogeneous distribution leading to much higher conductivity values and a substantially lower percolation threshold. The origin of the enhancement mechanism is proven in the present study by investigations using Infrared-Spectroscopy, contact angle measurements, interfacial tension analysis and optical microscopy and is related to a guided electrical percolation that takes place in segregated domains of stearic acid formed by shear-induced coalescence. Our finding reveals thus a novel approach to obtain a more efficient electrical percolation that greatly enhances the electromagnetic interference shielding effectiveness of functional composite materials.

Keywords: electromagnetic interference shielding, electrical conductivity, conductive composites, electrical percolation, metallic fillers.

1. Introduction

The recent decades have witnessed the rapid development of electronics and remote communications, the latter relying on the emission and reception of electromagnetic (EM) waves. One consequence is the dramatic increase in environmental EM pollution. Though a priori harmless to mankind, this EM pollution can have serious consequences on sensitive electronic devices (pacemakers, plane guidance systems, radars, etc.) such as for instance system dysfunction and breakdown. This topic is even more crucial in in-vehicle systems where wave emitters and receptors are stacked in a confined space, making them likely to interfere one with each other. Metallic plaques, films or meshes are today the most used approaches to shield electronics or cables from environmental EM pollution or to isolate an EM emitting device from its neighbors. These materials, however, suffer from their high cost, corrosion sensitivity and high density, making them not an optimal choice for light vehicles with reduced greenhouse gas emissions.

A promising alternative is the use of light conductive polymer composites with electromagnetic interference (EMI) shielding properties. This type of materials has drawn great interest for research and development, as testifies the great number of studies and literature reviews on the subject [1–4]. The choice of polymers is wide: thermoplastic resins such as polypropylene PP, PA, PC, PLA or PVDF or thermoset resins such as epoxy resins, PDMS or PU. The electrical conductivity of composite materials has been identified as one of the main parameters required to obtain high EMI shielding effectiveness (EMISE) [3,5]. Materials with a conductivity value below 10^{-10} S/m are usually considered insulating, between 10^{-10} and 10^{-7} S/m the material is suitable for antistatic applications, between 10^{-7} and 1 S/m for electrostatic discharge dissipation and above 1 S/m for EMI shielding. To reach this high value for electrical

conductivity and obtain thereby EMI shielding properties, the polymer matrices are usually mixed with micro- or nanofillers in order to get conductive composites and nanocomposites.

Carbon based materials are an attractive choice for fillers as they display good electronic conductivity combined with a low density. Examples of carbon-based fillers for EMI shielding are conductive polymers [6], carbon black [7,8], carbon fibers [9], carbon nanotubes (CNT) [10–12] and graphene [13,14]. Metallic fillers are also widely used due to their intrinsic conductivity that can lead to enhanced shielding properties. Steel fibers [15], nickel or silver nanoparticles [16,17], iron nanocrystals [18], copper nanowires [19–21] and even liquid metal [22] are examples of fillers of metallic nature. The use of fillers of high density can however lead to heavy composite materials [16]. Lately, much attention has been drawn to composites exhibiting great EMI shielding properties based on MXnes (2D inorganic fillers consisting of layers of transition metal carbides, nitrides or carbonitrides [23–25]). Ryu et al. recently measured an EMI shielding slightly below 40 dB at a frequency of 8 GHz with a sample thickness of 2 mm using PC/ABS composite materials filled with 20 phr carbon fibers [9]. Similar shielding properties at 8 GHz and 1 mm thickness have been reported in one of our previous studies [12] on PP-based composites filled with 7.5 vol% (15 wt%) carbon nanotubes. By trapping liquid eutectic GaIn in thermoset PDMS filaments arranged into a mesh, Wang et al. measured a shielding value of 50 dB at 3 mm thickness and 8 GHz [22]. Due to their limited intrinsic conductivity compared to metallic fillers, carbon-based fillers often lead to lower shielding properties at a given shield thickness, unless the volume fraction of fillers is increased [12]. This, however, can have negative consequences on composite processing. Several strategies exist to tackle this problem. A first one is combining different fillers in one polymer matrix to obtain a synergetic effect: the combination of different fillers can lead to a higher shielding effectiveness than composite materials prepared using only one type of filler [26–29]. A second possible strategy relies on filler segregation: the conductive fillers can be segregated

in one (percolated) phase of the composite material while the other phase does not contain any fillers [30–33]. Foaming is also reported to enhance the EMI shielding by a guided percolation phenomenon [15,28,34]. While being able to increase the electrical conductivity and EMI shielding properties of composites without increasing the filler loading, the fillers segregation strategy can have dramatic effects on the composite mechanical properties such as for instance elongation at break and shock resistance [32,33].

To solve these multiple challenges, much interest has been drawn on hybrid fillers that can exhibit large aspect ratios, leading to low percolation thresholds, high conductivities and low densities. These hybrid fillers-based composites show enhanced EMI shielding properties with a reduced among of fillers, leading thereby to composite materials of low density [35–37]. Light Silver-coated particles and fibers are effective fillers due to the conductivity of silver that is the highest of all metals [38], leading thus to composite materials with high EMI shielding properties [39–42]. Zeng et al. measured a shielding of more than 60 dB at 2 mm thickness and 8 GHz for PDMS filled with 0.3 vol% of Ag-PVP nanowires [39]. By coating cotton fibers with silver, Tan et al. obtained an impressive shielding value of 71 dB at 0.5 mm thickness and 8 GHz for 1.61 vol% silver content in a non-woven fabric [40]. Light hybrid silver-coated fibers have therefore great potential as fillers for light composite materials with enhanced conductivity and EMI shielding properties.

One of the crucial challenges in developing conductive polymer composites for EMI shielding applications is obtaining enhanced conductive and shielding properties without increasing the filler loading. This is because increasing the filler loading leads to higher densities (and consequently heavier materials), higher costs, a material processing that is becoming more difficult and degradation of mechanical properties. Here we report that, at a constant filler loading, the electromagnetic interference effectiveness of PP-based composite materials filled with metallic fillers can be increased by more than 60 dB by a phenomenon of

guided electrical percolation. Materials that have initially no electromagnetic shielding properties display a shielding effectiveness as high as 70 dB as a result of an electrical percolation taking place in segregated domains of stearic acid formed by shear-induced coalescence. Guiding the electrical percolation of fillers represents thus a very efficient approach to greatly enhance the electromagnetic shielding properties of functional composite materials.

2. Materials and methods

2.1 Materials

Polypropylene PP 7060 (density of 0.905 $g.cm^{-3}$, MFI index of 12g/10min, melting point T_m of 165°C) supplied by Total S.A. was used as a polymer matrix in this study. Tin microparticles (density of 7.29 $g.cm^{-3}$, melting point T_m of 231°C) were purchased from GoodFellow. The average particles diameter was 45 μm. Silver-coated glass microfibers were purchased from Hart Materials UK (Grade SG180 FB20). They are characterized by a silver content of 20 wt%, an average length of 180 μm, an average diameter of 15 μm and a density of 2.8 $g.cm^{-3}$. Stearic acid flakes (melting point T_m of 67-72°C, reagent grade, 95% purity) was purchased from Sigma-Aldrich-Merck. Tables 1 summarizes some of the physical and chemical properties of stearic acid.

Table 1: *Some physical and chemical properties of stearic acid* [45]

Chemical formula	**Melting point (°C)**	**Boiling point (°C)**	**Density at RT ($kg.m^{-3}$)**	**Solubility in water at RT ($mg.L^{-1}$)**	**Solubility in PP at 200°C**	**Surface tension at 70°C ($mN.m^{-1}$)**	**Electrical conductivity ($S.cm^{-1}$)**
$C_{18}H_{36}O_2$	69.6	282.4	837.4	3	Poorly soluble	28.2	10^{-11} Insulating

2.2 Fabrication of PP composites filled with PP – Tin microparticles and Ag-coated glass microfibers

PP composites based on Tin microparticles and Ag-coated glass microfibers were fabricated using the melt blending method. PP 7060 was mixed with the fillers and the stearic acid using an internal mixer (Thermoscientific Polylab OS RheoDrive 7 Haake, tank of 69 cm^3, roller rotors). Polymer pellets were first introduced in the mixer at low 20 rpm mixing speed, then fillers and stearic acid were added once the polymer resin was molten. For Tin microparticles, mixer temperature was set to 190°C and the compounds were mixed at 30 rpm for 10 mins and at 50 rpm for 3 mins. These processing conditions were chosen to prevent particles overheating and melting. For Ag-coated glass microfibers, the mixing was made at 200°C and 50 rpm for 6 mins and at 100 rpm for 4 mins. Concentrations between 3 and 30 vol% for the Tin particles and between 0 and 15 vol% for the stearic acid were employed. The torque applied on mixer rotors was recorded during the mixing process. After mixing, the obtained composites were frozen under liquid nitrogen and pelletized using a grinder (Pulverisette 19). The obtained pellets were hot pressed at 200°C and 250 bar into plaques and discs of 1 or 2 mm thickness, using a press (Servitec Polystat 200 T).

2.3 Electrical characterization of composites

In order to measure the electrical conductivity of the PP composites, plaques of *50* mm x *75* mm x *1* mm were measured along the direction parallel to the sample surface (thus, in the same direction as the electric field of the electromagnetic wave passing through the samples). The electrical contacts were gold metallized to eliminate the influence of the contact resistance. The DC electrical conductivity was measured with a Novocontrol Alpha Broadband Dielectric/Impedance Spectrometer and a Fluke 289 multimeter. Four samples of each composition were measured to check the experimental reproducibility.

2.4 Broadband EMI shielding measurements of composites

The electromagnetic interference shielding effectiveness (EMISE) of PP composites was measured using an Anritsu Shockline 2 ports VNA (MS 46522B) and two types of measurement cells (Fig. 1). The fundamental difference between these two measurement methods is related to the measurement mode: the coaxial method corresponds to the TEM mode simulating the far-field propagation of plane waves, while the measurements by waveguide correspond to the TE mode where only the electrical field is perpendicular to the propagation direction (but not the magnetic field). The TEM mode is thus not accessible using the waveguide method, which means that the measurements by waveguides do not correspond to free-space propagation of plane electromagnetic waves.

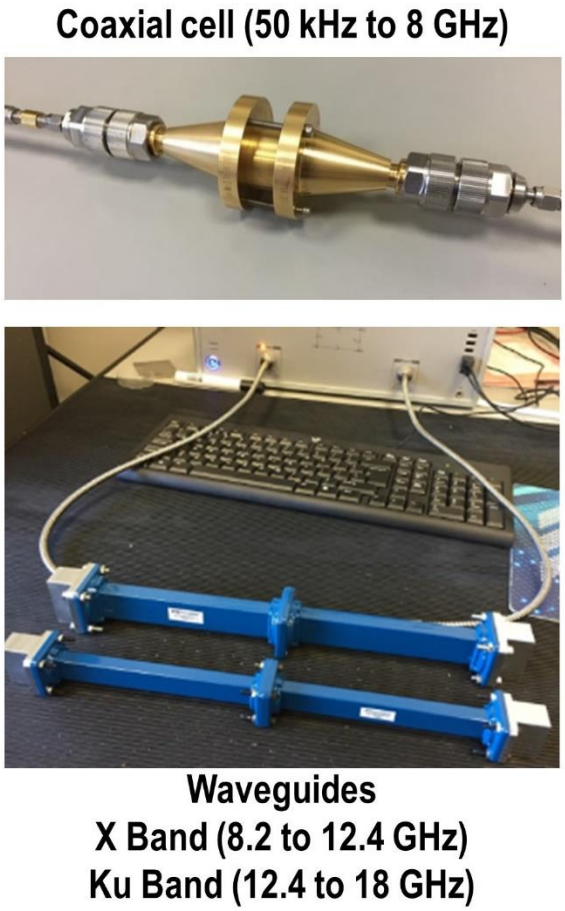

Fig. 1: coaxial cell (upper figure) and waveguides (lower figure) used for measuring the electromagnetic interference shielding effectiveness of composite materials.

From 50 kHz to 8 GHz, a coaxial cell has been employed (EpsiMu Multiwave PE 13 mm). For this cell, ring-shaped samples have been used and electrical contacts between the cell and the sample were gold metallized. Between 8.2 and 12.4 GHz (X band) and between 12.4 and 18 GHz (K_u band), two waveguide cells have been employed (Pasternack PE-W90S001-6 1701 and PE-W62S001-6 1650). For these waveguide cells, the samples were in the form of plaques fitting in the waveguides. Experimental setups are described in a previous work [12]. EMI shielding properties of PP composite filled with Ag-coated glass microfibers were measured on 1 mm-thick samples. The EMI shielding properties of PP composites prepared using Tin particles were measured on 2 mm-thick samples. Four samples of each composition

were measured to check the experimental reproducibility. The power was set to 0 dBm, which corresponds to 1 mW, and each point was the average of 5 measurements.

The total shielding effectiveness SE_T, the reflection shielding SE_R and the absorption shielding SE_A were calculated from the measured S-parameters S_{11} and S_{21} [1,5], as follows:

$$\boldsymbol{R = \left|S_{11}^2\right|} \quad (1)$$

$$\boldsymbol{T = \left|S_{21}^2\right|} \quad (2)$$

$$\boldsymbol{SE_T = -\log_{10}(T)} \quad (3)$$

$$\boldsymbol{SE_R = -\log_{10}(1 - R)} \quad (4)$$

$$\boldsymbol{SE_T = -\log_{10}\left(\frac{T}{1-R}\right)} \quad (5)$$

$$\boldsymbol{SE_T = SE_R + SE_A} \quad (6)$$

The EMI shielding effectiveness (EMISE) of a given shield is defined as:

$$\boldsymbol{SE = -10\log_{10}\left(\frac{P_t}{P_i}\right) = -20\log_{10}\left(\frac{E_t}{E_i}\right) = -20\log_{10}\left(\frac{H_t}{H_i}\right)} \quad (7)$$

P_i, E_i and H_i are the power, electric field amplitude and magnetic field amplitude of the incident EM wave, respectively, and P_t, E_t and H_t the power and electrical and magnetic field amplitudes of the EM wave transmitted through the shield. The shielding effectiveness is expressed in dB: while at 10 dB 90% of the incident wave power is blocked by the shield, at 40 dB it is 99.99% of the wave power that is shielded. In general, a shielding value of 30–40 dB is demanded for commercial applications, but higher shielding values are usually required for aeronautical or military applications.

When an EM wave falls onto the surface of given material (Fig. 2), a part of the wave is directly reflected at the first air-material interface due to a discontinuity in the EM wave impedance [5,46]. The matter is defined as:

$$\boldsymbol{Z} = \frac{\boldsymbol{E}}{\boldsymbol{H}} = \sqrt{\frac{\boldsymbol{\mu^*}}{\boldsymbol{\varepsilon^*}}} = \sqrt{\frac{\boldsymbol{j\omega\mu'}}{\boldsymbol{\sigma + j\omega\varepsilon'}}} \quad (8)$$

where E is the electric field and H the magnetic field of the EM wave in the material. μ^* and ε^* are the complex magnetic permeability and dielectric permittivity of the material. ω is the angular frequency of the wave ($\omega = 2\pi f$, f the wave frequency), μ' and ε' are the real part of the permeability and permittivity, respectively, σ is the electronic conductivity and j the imaginary number $\sqrt{-1}$. The wave impedance of vacuum (and air) is a constant equal to $Z_0 = \sqrt{\mu_0/\varepsilon_0} \approx 377\ \Omega$. The bigger the difference is between the air impedance Z_0 and the wave impedance Z, the more important will be the phenomenon of single reflection. Then, a part of the wave penetrates the shield and undergoes electromagnetic absorption all the way through the thickness of the shield due to induced current dissipation, dielectric polarization, interfacial polarization, eddy current dissipation, hysteresis loss and magnetic resonance loss [47]. These phenomena are described by a characteristic absorption length, also called skin depth [5,47]:

$$\boldsymbol{\delta} = \sqrt{\frac{\boldsymbol{2}}{\boldsymbol{\mu'\omega\sigma}}} = \sqrt{\frac{\boldsymbol{1}}{\boldsymbol{\mu'\pi f\sigma}}} \quad (9)$$

When passing through a length of δ, the EM wave loses 63% of its amplitude due to absorption. According to eq. 9, absorption is more important at higher frequencies and for higher conductivity values or when magnetic materials are employed.

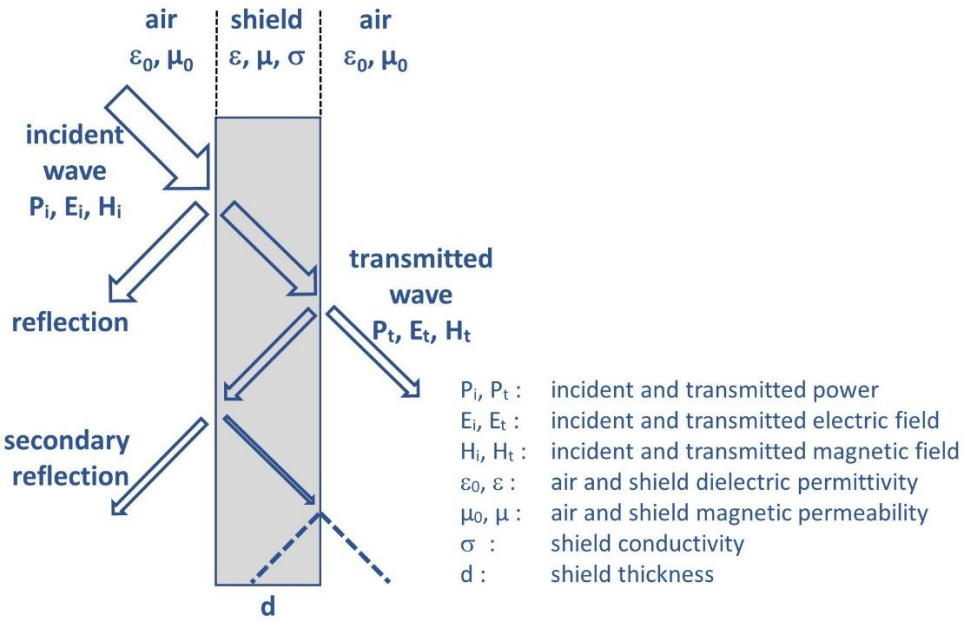

Fig. 2: schematic representation of the electromagnetic interference shielding mechanisms.

A third shielding mechanism at play is related to multiple internal reflections. As the EM wave reaches the second rear material-air interface, a part of the wave goes through but the other part is reflected back to the first interface. On the way back it undergoes absorption again, gets transmitted and reflected at the first air-material interface and goes back to the second rear interface. Thus, the EM wave passes several times between the two air-materials interfaces, with an amplitude that decreases at each passage. These three shielding mechanisms and their impact on total EMI shielding of a material were treated in detail in a previous study and led to the general EMISE formula for a homogeneous and isotropic material [12]:

$$\boldsymbol{SE_T = SE_A + SE_R + SE_M} \tag{10}$$

$$\boldsymbol{SE_A = 20.\frac{d}{\delta}\log_{10}(e)} \tag{11}$$

$$\boldsymbol{SE_R = -20.\log_{10}\left(\left|\frac{4.Z_0.Z}{(Z+Z_0)^2}\right|\right)} \tag{12}$$

$$SE_M = 20.\log_{10}\left(\left|1 - \left(\frac{Z-Z_0}{Z+Z_0}e^{-d/\delta}\right)^2\right|\right) \quad (13)$$

$$f_c = \frac{1}{\pi\mu'\sigma d^2} \quad (14)$$

where |.| is the absolute value of a complex number and d the shield thickness. At low frequencies (lower than the absorption characteristic frequency f_c [5]) EMI shielding is constant and depends solely on the composite conductivity and thickness. Above f_c, shielding increases rapidly with frequency because of wave absorption. Thus, for homogeneous and isotropic materials (non-magnetic) the main parameters having a significant impact on EMI shielding are the material electrical conductivity, the thickness and the frequency of the incident wave.

2.5 Optical microscopy

For optical observation, PP composites were cut in thin layers of 20 and 50 µm thickness using a Leica RM2265 microtome. Microscopy observations were made using an Olympus BX 41 microscope coupled with an Olympus DP 26 camera. Lens of magnification x4, x10 and x20 were used. Image analysis was done using the CellSensEntry software.

2.6 Transmission Infrared spectroscopy on filler – stearic acid mixes

Different ratios of Tin particles and stearic acid, and Ag-coated glass fibers and stearic acid were put in a beaker, heated 10 mins at 100°C in an oven and mixed vigorously with a spatula for 5 minutes. 2.5 mg of each of these blends (cooled down to room temperature) were grinded with 197.5 mg of KBr powder, introduced in a hydraulic press and pressed into thin disks between two mirror-smooth plates. Transmission infrared spectroscopy measurements were carried out using a Thermoscientific iS-10 spectroscope. The sample discs were measured

at wavelengths ranging from 1000 to 4000 cm^{-1} using a detector cooled with liquid nitrogen. A background spectrum with an empty chamber was measured prior to sample measurements. For each compound ratio, three different samples were measured and the final curve was the average of three experimentally measured curves.

2.7 Contact angle measurement on filler – stearic acid mixes

Several grams of the Tin particles and Ag-coated glass fibers previously blended with the stearic acid at 100°C were introduced in a hydraulic press and pressed between two mirror-smooth surfaces. Small discs with a smooth surface were obtained. Contact angle measurements were made using a Kruss Easydrop experimental setup coupled with a Hamilton 500 µL syringe and an Allied Vision Technology Stinray camera. A 1 µL deionized water droplet was placed on the surface of the disks. Once the drop was stabilized, a picture was taken and analyzed with the Drop Shape Analysis software that automatically measures contact angles. For each compound ratio, ten water drops distributed over three different samples were measured to validate experimental reproducibility.

2.8 Transmission infrared microscopy

Transmission infrared microscopy was used to investigate the distribution of the stearic acid in the PP/Tin particles composites. Microtome cut layers of 20 µm thickness were measured to insure good beam transmission through the sample. A Thermoscientific Nicolet iN 10 MX infrared microscope in transmission mode was used to carry-out these measurements. Samples were placed on a pressed disk of pure KBr of 1 mm thickness and inserted in the dry microscope chamber. A window of 20 x 20 μm^2 was probed in order to differentiate particles

concentrated domains (called particles domains) and domains with a deficit of particles (called polymer domain). The measurements were carried-out at wavelengths ranging from 1000 to 3500 cm^{-1} using a liquid nitrogen cooled detector (256 scans, high spectral resolution). For each composite, three polymer domains and three particles domains were measured on three different samples (nine spectra for each domain type) to validate the experimental reproducibility. Around the stearic acid peak at 1710 cm^{-1}, the spectral area under the curve was measured between 1680 and 1740 cm^{-1} using a baseline correction relying on spectra measured on composites free of stearic acid.

3. Results and discussion

3.1 Electrical conductivity of PP composites

The electrical conductivity values of PP composites are displayed in Figure 3. Fig. 3-a shows the electrical properties of the composites prepared using Tin particles. In dependence on the particles volume fraction, the composite conductivity goes from 10^{-8} S/m to more than 10^{4} S/m. For composites prepared without the addition of stearic acid (filled dots), the material is insulating up to a filler concentration of 15 vol% and reaches a conductivity of 870 S/m at 30 vol% of particles. The concentration where the composite materials go from insulating to conductive properties, called the percolation threshold, is an important parameter in the study of conductive materials [48]. A reduced percolation threshold corresponds to conductive composited with a lower filler content, which can be of great advantage to conserve good mechanical properties and a low density. The addition of stearic acid into the PP/Tin composites (1 vol% of stearic acid per 5 vol% of particles) has a two-fold positive effect. The first effect is a percolation threshold that is considerably lowered, from 15 vol% to 7 vol%. In this range of

filler concentration, composites that were insulating in the absence of stearic acid become conductive when the stearic acid is added during the melt blending process.

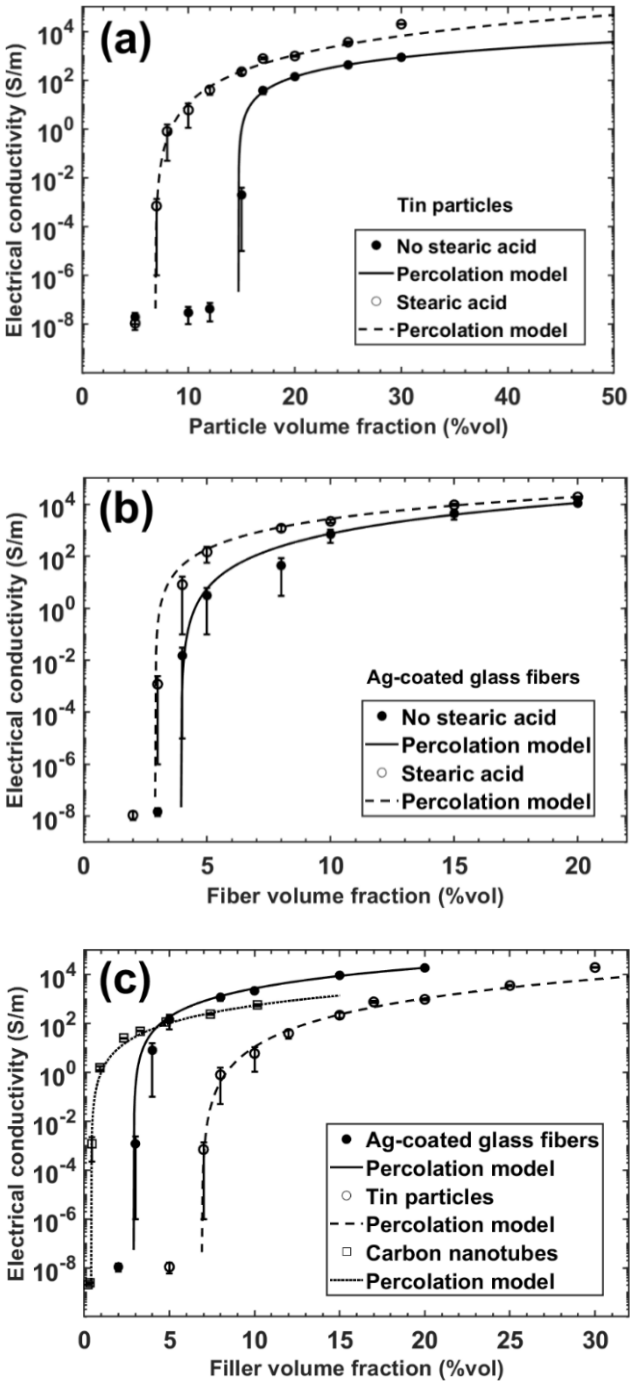

Fig. 3: *Electrical conductivity of PP/Tin particles and PP/Ag-coated glass microfibers composites. (a) Conductivity of PP/Tin composites with and without stearic acid as a function*

of the particle volume fraction (1 vol% of stearic acid per 5 vol% particles). Continuous lines are fitted curves using the theoretical percolation law. (b) Same as before with Ag-coated glass microfibers. (c) Comparison with the PP/CNT composite materials from a previous work [12].

The other positive effect brought by the addition of the stearic acid is the increased conductivity on the saturation plateau of the percolation curve. Thus, for 20 vol% and 30 vol% particle concentration, the conductivity increased from 140 to 1000 S/m and from 870 to 20,000 S/m, respectively, by adding the stearic acid. It is worth mentioning that the stearic acid has a negligible conductivity value [45], consequently, the increased conductivity obtained with the addition of the stearic acid cannot be attributed to an increasing conductive content. Stearic acid is a saturated fatty acid with amphiphilic properties due to its carboxyl chemical head and long carbon tail. It can be fabricated artificially but is mainly obtained by splitting natural fats and oils. Sunflower oil, beef tallow and cocoa butter are great sources of stearic acid [45]. Thanks to their properties, fatty acids are often used in the processing and cosmetic industries. Their ability to interact and react with inorganic and metallic surfaces can improve filler dispersion and stabilization in a polymer matrix as well as composite processability due to their lubricating effects [43,44,49,50]. Addition of stearic acid in composites containing conductive fillers was reported to improve the mechanical, dielectric and conductive properties as well as the EMI shielding properties [51–55]. Xiong et al. observed a decrease in the electrical resistivity from 10^{10} Ω.cm to less than 10^{6} Ω.cm when adding 11.5 vol% of stearic acid to a PU-based composite filled with 6.5 vol% carbon black fillers [56]. Vanga-Bouanga et al. noticed the same phenomena in a HDPE/ polyaniline composite where the electrical conductivity at 10 wt% PANI increased from 3.3 x 10^{-17} S/cm to 7.3 x 10^{-10} S/cm when adding 1 wt% stearic acid [57]. These results are thus in agreement with the results reported in the present study.

The experimental points can be fitted with the empirical percolation law proposed by Kirkpatrick [48]:

$$\boldsymbol{\sigma = \sigma_0(\varphi - \varphi_c)^t \quad with\ \varphi > \varphi_c} \tag{15}$$

where σ is the composite conductivity, σ_0 is a constant related to the intrinsic conductivity of fillers and t a critical exponent dependent on the dimensionality of the conductive network. Fitting parameters are listed in Table 2.

Table 2: *Fitting parameters according to Eq. 15 for PP composites with and without stearic acid. R is the determination coefficient.*

Filler	**Stearic acid (vol%)**	ϕ_c	σ_0 **(S/m)**	t	R^2
Tin particles	0	0.147	2.16×10^4	1.72	0.9961
	1 per 5 vol% particles	0.069	6.83×10^5	3.17	0.9413
Ag-coated glass fibers	0	0.0395	1.81×10^6	2.7	0.9953
	1 per 5 vol% fibers	0.029	9.44×10^5	2.2	0.9986

Conductivity values obtained for PP/Tin composites are lower than the intrinsic conductivity reported for Tin (9.17×10^6 S.m^{-1}) [38]. This can be attributed to the contact resistance between the Tin particles that reduces the global composite conductivity. The conductivity values are higher in the presence of stearic acid, suggesting that, for a fixed amount of fillers, the electrical contacts between the particles are better or more numerous. The critical

exponent parameter *t* is close to 2 in the absence of stearic acid, suggesting a 3D homogeneous percolation. With the addition of stearic acid, this parameter is higher (= 3.17), suggesting a non-homogeneous 3D percolation. Exponent parameters higher than 2 are often found in segregated structures [20,30,58]. This indicates filler segregating effects taking place in the presence of the stearic acid. Similarly to PP/Tin composites, the composite materials prepared using Silver-coated glass microfibers are insulating at low filler loading and become conductive when the percolation threshold is reached. The experimental points can be fitted by the percolation law expressed by (Eq. 15). The estimated percolation thresholds are thus 3.95 vol% without stearic acid and 2.9 vol% with the stearic acid. The intrinsic electrical conductivity of silver is 6.3 x 10^7 $S.m^{-1}$ [38], higher than the conductivity values obtained for our composite materials. This originates from a non-negligible contact resistance between the microfibers. Values close to 2 are obtained for the critical exponent *t*, suggesting a homogeneous 3D percolation [48].

In Fig. 3-c, the electrical properties of PP/Tin and PP/Ag composites with stearic acid (1 vol% of stearic acid per 5 vol% of filler) are compared to the conductivity of CNT-based composites from our previous study [12] where the same polymer matrix was used to prepared the composite materials. The lowest percolation threshold is obtained with the CNT composites (0.4 vol%), but the highest conductivities are reached using metallic fillers. The composites prepared with the Silver-coated glass microfibers constitute thus a good compromise between a low percolation threshold/medium conductivity obtained with the CNT-based composites and high percolation threshold/high conductivity observed when Tin particles were used as fillers. Consequently, PP-based composites prepared using Ag-coated microfibers exhibit higher conductivity values than CNT-based composites and a lower percolation threshold as compared to composites prepared using Tin particles.

The conductivity of the PP composites prepared using the two types of fillers is shown in Fig. 4, as a function of the volume fraction of the stearic acid. At 15 vol% Tin particles (Fig. 4-a), conductivity increases considerably even with the addition of 0.2 vol% of stearic acid. The large increase from 0.002 S/m for composites prepared without the addition of stearic acid to 2600 S/m with the addition of 10 vol% stearic acid can be explained by the fact that the 15 vol% particles concentration is very close to the percolation threshold. The increase is comparatively less important at 20 vol% particle since the composite material is already well percolated.

It can be noted that, for 15 vol% Tin particles, conductivity decreases at 15 vol% stearic acid as compared to 10 vol% stearic acid. An excess of stearic acid appears thus to be detrimental to the composite electrical properties. Similarly, for composites filled with Ag-coated glass microfibers (Fig. 4-b) the conductivity increases with increasing the volume fraction of stearic acid. At 8 and 10 vol% of Ag-coated glass fibers, conductivity goes from 44 S/m without stearic acid to 1200 S/m when adding 2 vol% of stearic acid and from 700 S/m to 2200 S/m, respectively. A maximal value of 1.4×10^4 S/m was reached for 20 vol% Ag-coated microfibers upon adding 1.5 vol% stearic acid. Conductivity seems to decrease at higher fractions of stearic acid, indicated, as also observed for the Tin particles, a detrimental effect caused by excess.

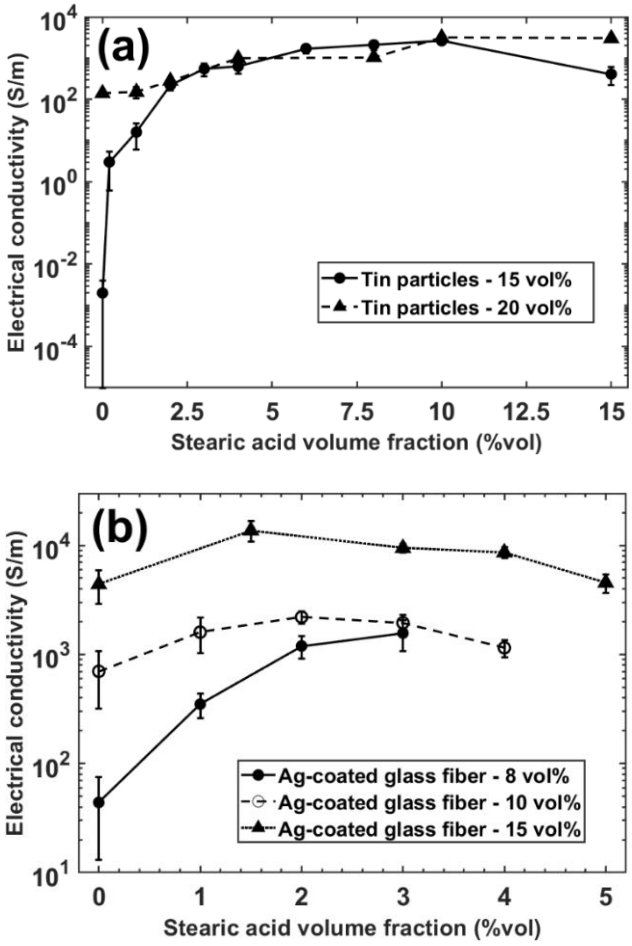

Fig. 4: *Composite conductivity as a function of the volume fraction of stearic acid. (a) PP/ Tin composites at 15 and 20 vol% Tin particles. (b) PP/Ag-coated glass microfibers composites at 8, 10 and 15 vol% microfibers.*

High conductivities using metallic fillers were also reported in several other studies. Duan et al. measured a conductivity value of 2648 S/m for 2.58 vol% of Nickel particles dispersed in a UHMWPE polymer matrix [17]. Coating cotton fibers with 2.6 µm-thick layer of Silver nanoparticles, Gao et al. measured a conductivity value of 9.8 x 10^5 S/m on non-woven fabric [21].

3.2 EMI shielding properties of PP composites measured in coaxial cell

The high conductivity values measured on our PP composites give them a great EMI shielding potential. Indeed, according to Eqs. 10–13, increasing the composite conductivity leads to an enhancement in the shielding effectiveness. The EMI shielding properties measured from 100 kHz to 8 GHz using the coaxial cell method for PP/Tin microparticles and PP/Silver-coated glass microfibers composites prepared without the addition of stearic acid are shown in Figure 5-a and 5-b, respectively. The shielding effectiveness of PP/Tin composites is 0 dB at 15 vol% particles but reaches, at low frequencies, 31 dB and 48 dB at filler concentrations of 20 vol% and 30 vol%, respectively.

A drop of shielding effectiveness can be observed at high frequencies, attributed to an inductive impedance contribution that is known to lower the effective conductivity of metallic materials. This drop in EMI shielding with increasing frequency is also reported in numerous other studies dealing with metallic materials or composites filled with metallic fillers [59–66]. For instance, Lee et al. measured a drop of EMI shielding from 80 dB at 300 kHz to 60 dB at 12 GHz for a PS matrix filled with Copper coated polymer beads [59]. For a bamboo fabric coated with Silver and Nickel, Lu et al. observed a decrease in the shielding effectiveness from 54.5 dB at 30 MHz to 49 dB at 1 GHz [64].

Similar observations can be made for the PP/Ag-coated microfibers composites (Fig. 5-b): an increase in the global shielding effectiveness with increasing the volume fraction of fillers and a drop of the shielding effectiveness at high frequencies are observed. Shielding values of 40 dB and 65 dB at low frequencies are obtained with 10 and 20 vol% of microfibers, respectively, for a sample thickness of 1 mm. An increase in shielding effectiveness at high frequencies is observed for 20 vol% microfibers, suggesting the onset of absorption phenomena. The calculation of the value of the absorption characteristic frequency (Eq. 14 with σ = 11,000

S/m) gives f_c = 23 MHz which is in good agreement with the onset of the EMI absorption effects observed in the measured shielding spectra (Fig. 5b).

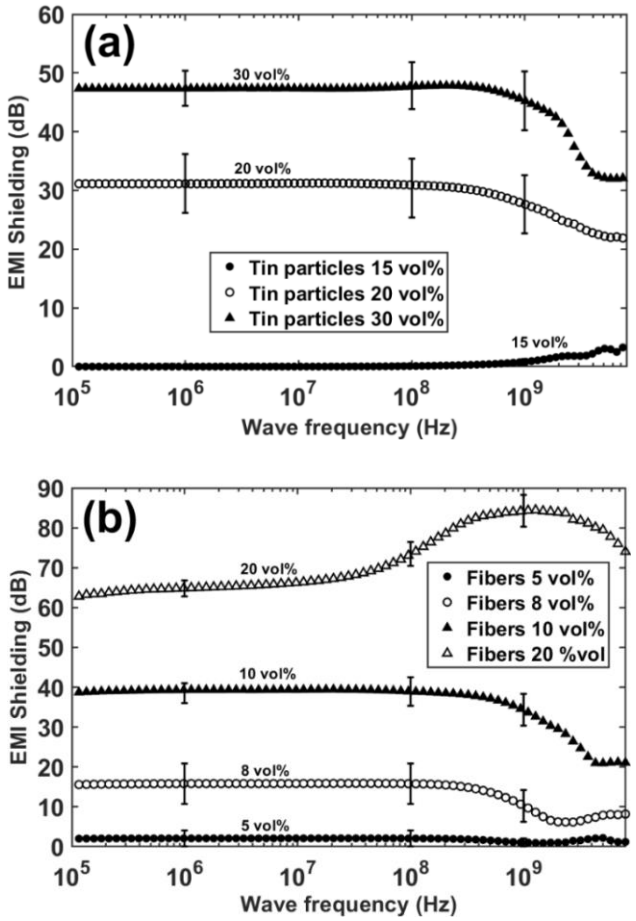

Fig. 5*: *Shielding effectiveness of (a) PP/Tin composites and (b) PP/Ag-coated glass fibers composites, as a function of frequency, measured by the coaxial method for different volume fractions of fillers. The sample thickness is 2 mm for PP/Tin composites and 1 mm for PP/Ag-coated microfibers composites.

As composite conductivity increases with increasing the concentration of stearic acid, EMI shielding follows the same behavior (Fig. 6). Fig. 6-a shows the measured shielding effectiveness of PP/15 vol% Tin composites (at 2 mm thickness), measured by the coaxial

method for different amounts of stearic acid added into the composite materials. The composite prepared using 15 vol% Tin particles without adding stearic acid exhibits no shielding properties whereas, upon adding 10 vol% of stearic acid, shielding values of 57 dB at low frequencies and 76 dB at 2 GHz are obtained. It is worth reminding the fact that stearic acid does not have any electrical conduction properties [45]. Similarly to the results that were previously discussed, a drop in the shielding effectiveness at high frequencies can be observed. For composites prepared using 3, 6, 8 and 10 vol% stearic acid, shielding effectiveness increases first with increasing frequency due to absorption phenomenon and then drops due to inductive effects. The characteristic frequencies fc related to the onset of absorption effects change in dependence on the addition of stearic acid. For instance, according to the results presented in Fig. 6a, absorption effects take place much earlier (thus, at lower frequencies) when the concentration of the stearic acid increases (i.e. at 8 vol% and 10 vol%). As explained in one of our recent articles [12], the characteristic frequency fc depends on the conductivity value: the higher the conductivity value, the earlier absorption effects take place (fc is thus shifted to lower frequencies). Absorption effects appear thus much earlier because, as shown in Fig. 4a, the conductivity of our composite materials increases with the addition of stearic acid. The calculated characteristic absorption frequencies according to (Eq. 14) match well the onset of absorption effects measured in the shielding spectra.

The composite shielding effectiveness as a function of the concentration of stearic acid for 15 vol% and 20 vol% Tin particles is displayed in Fig. 6-b and 6-c, for two frequencies: 1 MHz (low frequency where the wave reflection mechanism dominates the shielding) and 2 GHz (high frequency where reflection and absorption are predominant). For both particle concentrations the shielding increases with increasing the concentration of stearic acid. The drop in shielding observed at high frequencies due to inductive effects becomes significant starting with a frequency of 2 GHz.

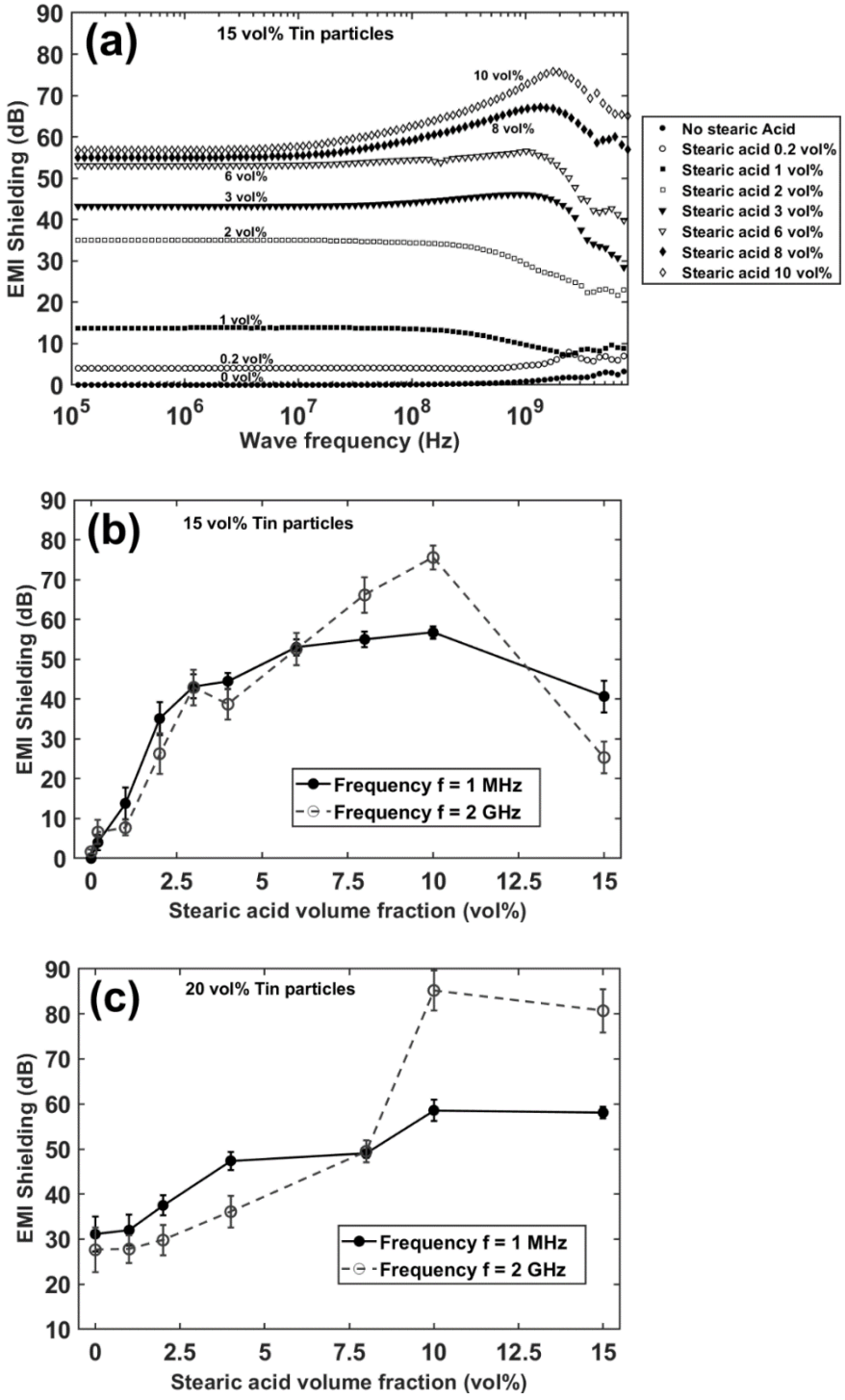

Fig. 6: *Shielding effectiveness measured using the coaxial cell for PP/Tin composites and 2 mm-thick samples: (a) as a function of frequency at 15 vol% Tin particles and different concentrations of stearic acid; (b) as a function of the concentration of stearic acid at 15 vol%*

Tin particles and frequencies of 1 MHz and 2 GHz; (c) as a function of the concentration of stearic acid at 20 vol% Tin particles and frequencies of 1 MHz and 2 GHz.

Similarly to the behavior observed for the conductivity, an excess of stearic acid has a negative impact on the shielding effectiveness. This phenomenon has been investigated and related to changes in the mixing conditions. Mixing shear forces were observed to dramatically drop when the stearic acid was added in excess (at 15 vol%), which corresponds to considerably lower torques during mixing. This lowered mixing shear is expected to lead to a less efficient dispersion of fillers, resulting in lower electrical and shielding properties. This effect can be attributed to the lubricating properties of stearic acid that can accumulate at the interface between the walls of the mixer tank and the composite material being mixed [44,50]. The mixing torque values for Tin particles-based composites are displayed in Figure S1 in the Supplementary Information Part.

As displayed in Figure 7, similar observations can be made for PP-based composites filled with Ag-coated glass microfibers: the addition of stearic acid has a positive impact on shielding for 10 vol% microfibers: the shielding effectiveness increases from 40 to 49 dB at 1 MHz and from 29.5 to 63 dB at 2 GHz when adding 2 vol% of stearic acid. The increase is particularly significant at high frequencies, where the addition of stearic acid appears to compensate the drop of shielding caused by inductive effects. It also appears to favor the onset of absorption effects. The characteristic absorption frequencies f_c expressed by (Eq. 14) match well the onset of absorption effects observed in the measured spectra. The shielding effectiveness as a function of the concentration of stearic acid for microfibers contents of 8, 10 and 15 vol% is displayed in Fig. 7-b and 7-c, for frequencies of 1 MHz and 2 GHz. Similarly to PP-based composites filled with Tin particles, the shielding effectiveness increases with increasing the concentration of stearic acid, reaching a value of 88 dB at 2 GHz for composites

with 15 vol% microfibers and 4 vol% stearic acid at 1 mm thickness. While shielding is lower at high frequencies than at low frequencies in the absence of stearic acid, this tendency reverses when stearic acid is added. For three different microfibers contents, an optimal concentration for stearic acid is observed: 2 vol% for 8 and 10 vol% fibers, and 4 vol% for 20 vol% fibers. The optimal concentration seems to be roughly proportional to the microfibers content (about 2 vol% stearic acid per 10 vol% microfibers). Above this optimal concentration, the composite shielding properties start to decrease. As for composites based on Tin particles, the composite mixing shear (related to the mixer measured torque) is observed to dramatically decrease at 4 vol% stearic acid. The torques measured for composites of PP/Silver-coated glass fibers/stearic acid are given in Figure S2 in the Supplementary Information Part. EMI shielding effectiveness and electrical conductivity of PP composites with and without stearic are listed in Table 3, for different filler contents. Shielding values as high as of 90 dB and 91 dB are reached with 30 %vol Tin particles composite (2mm thickness) and with 20 vol% Ag-coated glass fibers composite (1 mm thickness), respectively.

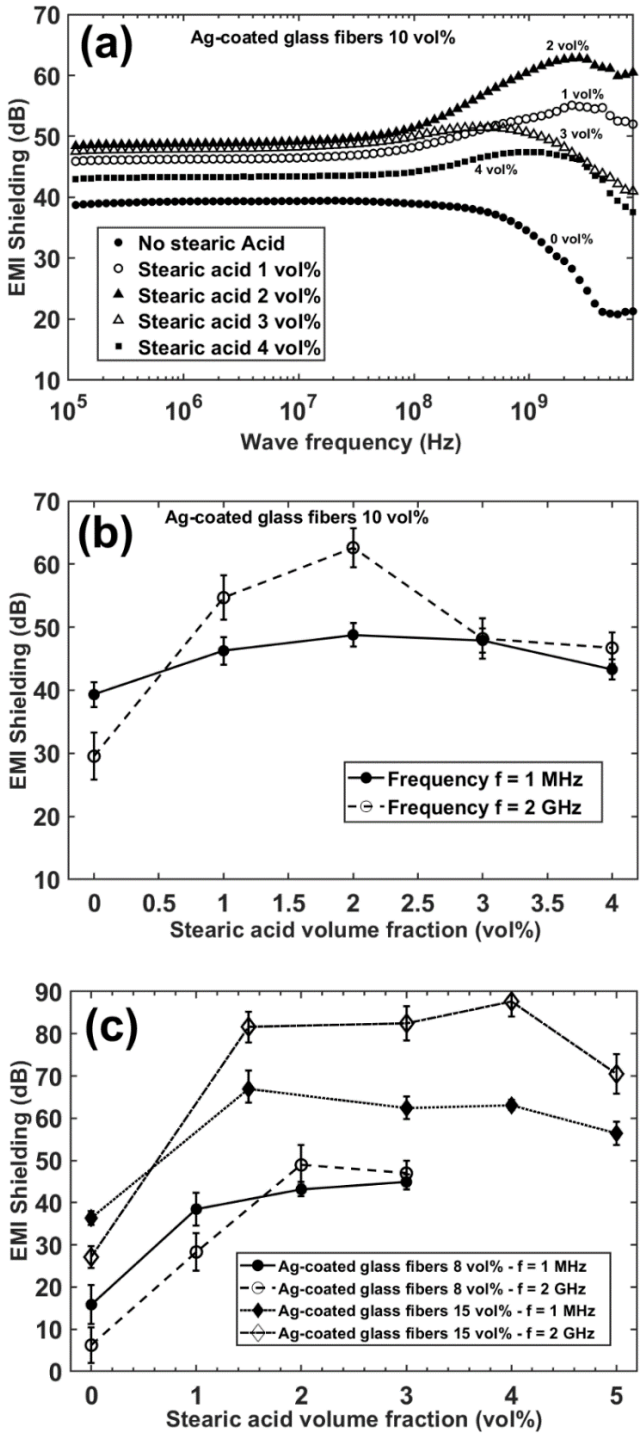

Fig. 7: *Shielding effectiveness measured by the coaxial method for composites of PP/Ag-coated glass fibers/stearic acid and 1 mm-thick samples. (a) as a function of frequency for different concentrations of stearic acid and 10 vol% microfibers. (b) as a function of the concentration of stearic acid at frequencies of 1 MHz and 2 GHz for 10 vol% microfibers. (c) as a function of*

the concentration of stearic acid at frequencies of 1 MHz and 2 GHz for 8 vol% and 15 vol% microfiber contents.

Table 3: *Measured electrical conductivity and EMI shielding of PP composites with and without addition of stearic acid. The samples are 2mm-thick for the composites prepared using Tin particles and 1 mm-thick for composites prepared using Ag-coated glass microfibers.*

Filler	**Filler vol%**	**Stearic acid vol%**	**Electrical conductivity (S/m)**	**EMI shielding at 1 MHz (dB)**	**EMI shielding at 2 GHz (dB)**
Tin particles	25	0	430 ± 20	43 ± 2	45 ± 2
		5	3600 ± 200	60 ± 3	65 ± 3
	30	0	870 ± 50	47 ± 2	42 ± 2
		6	19700 ± 700	74 ± 4	90 ± 5
Ag-coated glass fibers	5	0	3.1 ± 2	2.2 ± 1	1.1 ± 0.6
		1	100 ± 70	18 ± 3	9 ± 2
	20	0	11000 ± 1000	63 ± 2	84 ± 4
		4	19000 ± 1000	69 ± 2	91 ± 4

3.3 EMI shielding properties of PP composites measured by the waveguide method

The EMI shielding properties of the two composite materials measured from 8.2 to 18 GHz using the waveguide method are displayed in Figure 8. The experimental results of the two waveguides (8.2 – 12.4 GHz and 12.4 – 18 GHz) were reunited in the same graphs. The EMI shielding measured using waveguides as a function of frequency for composites prepared

using 15 vol% Tin particles and different amounts of stearic acid is presented in Fig. 8-a. Unlike the previous results measured with the coaxial cell, the shielding effectiveness measured in the absence of stearic acid is not zero, but close to an average of 20 dB for a thickness of 2mm. As indicated in Fig. 8-b, the concentration of stearic acid leading to an increase in shielding at 12 GHz seems to be situated in the range between 2 vol% and 6 vol%. For composites with 20 vol% Tin particles, a monotonic increase in shielding with the concentration of stearic acid is observed, with no decrease at high concentrations. At 10 vol% microfibers, the optimal stearic acid concentration is reached at 3 vol%, leading to a shielding value as high as 70 dB at 12 GHz and 1mm thickness. At 15 vol% fibers, the optimal concentration of stearic acid is 3 vol%, leading to shielding effectiveness as high as 88 dB.

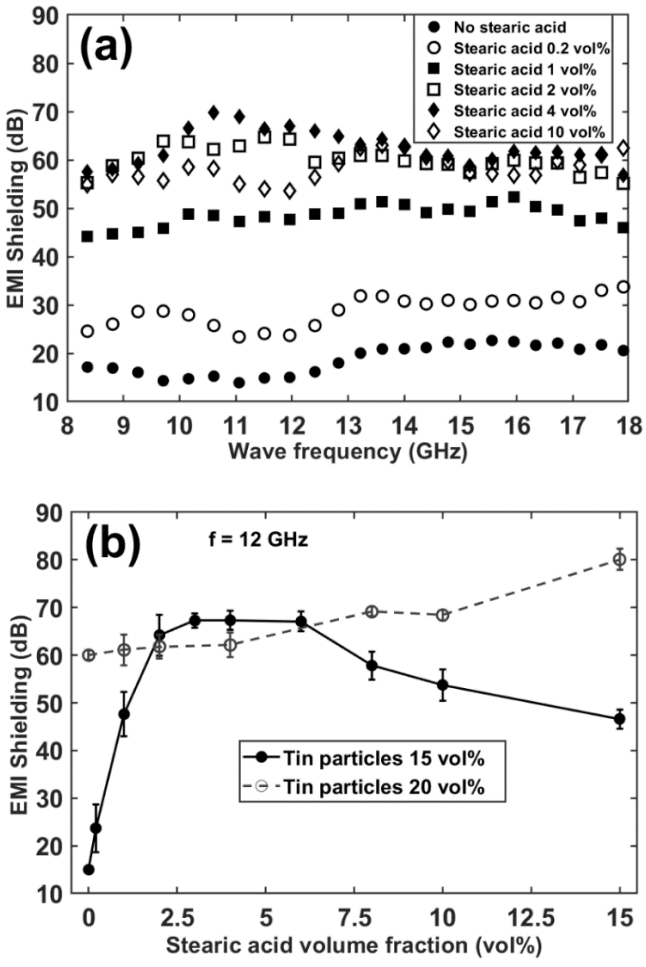

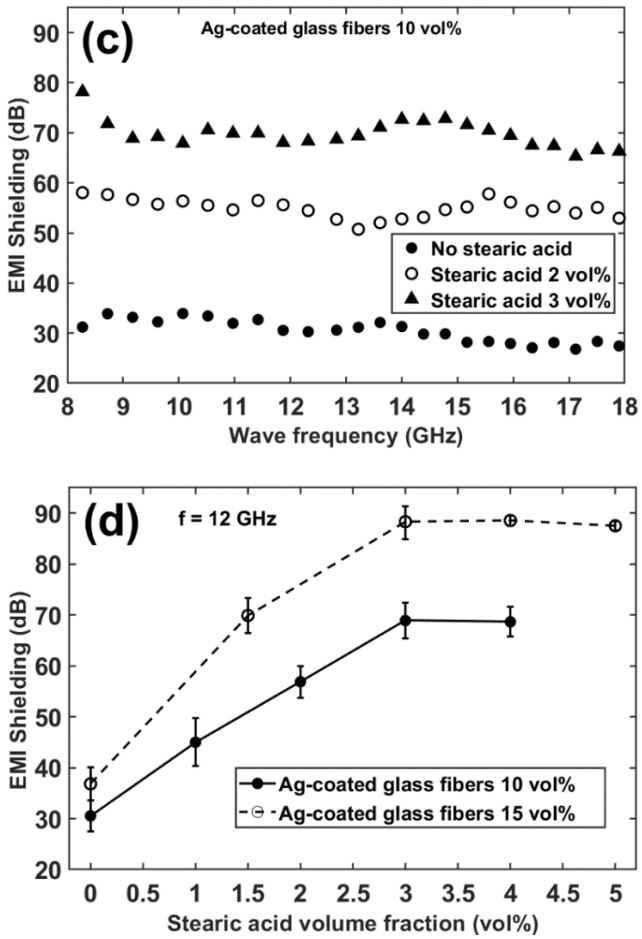

Fig. 8: *Shielding effectiveness measured in waveguides for PP/Tin particles and PP/Ag-coated microfibers composites. (a) as a function of frequency for different concentrations of stearic acid at 15 vol% Tin particles. The sample thickness was 2 mm. (b) as a function of the concentration of stearic acid at a frequency of 12 GHz, for 15 and 20 vol% Tin particles. (c) as a function of frequency for different concentrations of stearic acid and 10 vol% microfibers. The sample thickness was 1 mm. (d) as a function of the concentration of stearic acid at a frequency of 12 GHz, for 10 and 15 vol% microfibers.*

The conductivity values and the EMI shielding properties of the composites are listed in Table 4 and compared to other composites found in the literature.

Table 4: *Conductivity and EMI shielding properties in the X-band at 8.2 GHz of polymer composites found in the literature.*

Polymer matrix	**Filler**	**Filler content**	**σ (S/m)**	**EMI sample thickness (mm)**	**EMI shielding (dB)**	**Ref.**
PP	Tin particles*	15 vol%	2600	2	67	our work
PP	Ag-coated glass fibers*	10 vol%	2200	1	70	our work
PC / ABS	Carbon Fibers	20 phr	1050	2	40	[9]
PP	CNT	10 vol%	580	1	58	[12]
PU	Graphene	20 wt%	830	1.5	61	[67]
PP	Stainless steel fibers	1.5 vol%	0.1	3.1	40	[15]
Epoxy	MXenes	15 wt%	100	2	41	[25]
UHMWPE	Ni particles	2.58 vol%	2650	2	52	[17]
EMA / EOC	Cu nanowires	15 wt%	1000	1	45	[20]
PDMS	Liquid eGaIn	8.43 vol%	40 000	3	50	[22]
PDMS	Ag-PVP nanowires	0.26 vol%	1400	2	70	[39]

Epoxy	Ag-coated glass spheres	19 vol%	-	1.6	64	[41]
Epoxy	Ag-coated glass fibers	19 vol%	-	1.6	51	[41]
PLA	Ag-coated PLA fibers	5.8 vol%	254	1.5	49	[42]

*with stearic acid

Our composite materials also display good mechanical properties compared to CNT-based composites: at a constant 10 vol% filler content, the elongation at break is 12.3% compared to 3.8% for CNT-based composite. Density and tensile mechanical properties are displayed in Table S1 and Figure S3 in the Supplementary Information Part. Additionally, the impact of the stearic acid on the rheological properties of similar composite materials has been systematically investigated in one of our recent studies [88]. The rheological properties of pure steric acid are reported in [89]. According to this study, the shear viscosity of the stearic acid is Newtonian has a value close to 3 mPa.s.

3.4 Morphology of composites

The microscale morphology of our composite materials was investigated using optical microscopy in order to unravel the mechanisms underlying the enhancement in shielding properties observed upon addition of stearic acid. Optical images are shown in Figure 9. Using the microtome cutter, layers of 20 and 50 µm thickness have been made and investigated. Microscopic images taken on 20µm-thick composite layers for the composite with 15 vol% Tin particles with no stearic acid and with 6 vol% stearic acid are displayed in Fig. 9-a and 9-b.

This concentration of stearic acid was chosen because it gave the highest increase in electromagnetic properties.

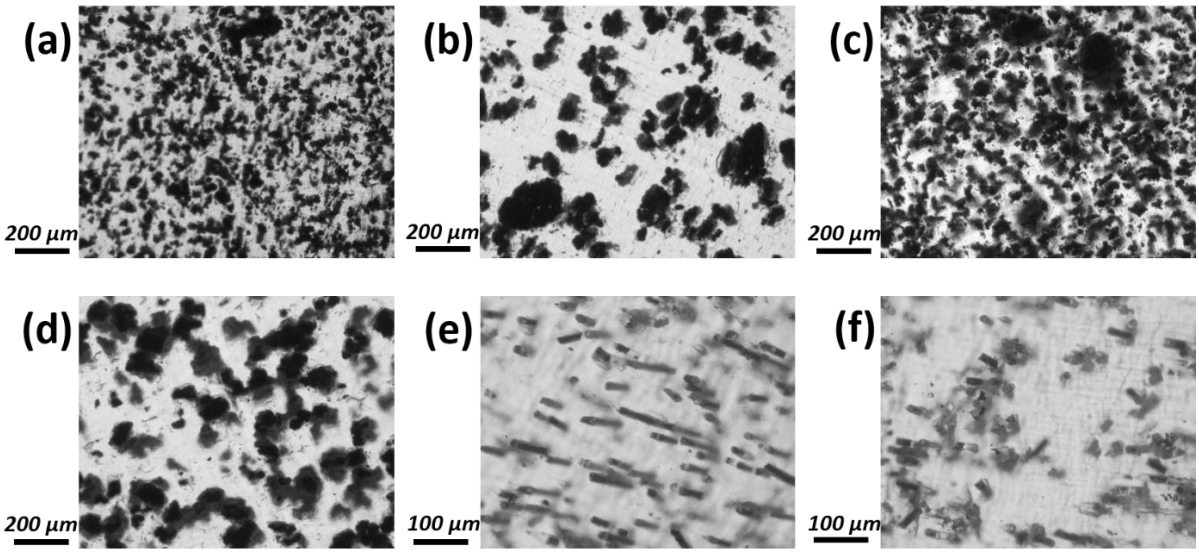

Fig. 9: *Optical microscopy images of the composites of PP/Tin particles and PP/Ag-coated glass microfibers.(a) 15 vol% Tin particles, 20 µm-thick sample, x10 magnification, no stearic acid. (b) Same as before but with 6 vol% stearic acid. (c) 15 vol% Tin particles, 50 µm-thick sample, x10 magnification, no stearic acid. (d) Same as before but with 6 vol% stearic acid. (e) 10 vol% Ag-coated glass fibers, 20 µm-thick sample, x20 magnification, no stearic acid. (f) Same as before but with 3 vol% stearic acid.*

The difference of morphology is striking: in the absence of stearic acid, the Tin particles are well dispersed in the PP matrix with little to no particles percolation. With the addition of stearic acid, the particles are aggregated with aggregates sizes comprised between 100 and 300 µm diameter. Areas between the aggregates – ranging from 100 µm to 400 µm in size – are relatively free of particles and constitute polymer domains.

At first glance, there seems to be few contacts between the aggregates, but a closer look at the image presented in Fig. 9-d that shows a thicker 50 µm layer indicates multiple contacts between the aggregates. These multiple contacts form a 3D network, explaining the conductive nature of this composite. At the same layer thickness (50 µm), composites prepared with no stearic acid show few to no particle/particle contacts. The addition of stearic acid has thus the effect of aggregating the particles, favoring particles percolation on the composite macroscale and improving thereby the electrical conductivity as well as the shielding properties. The observed morphologies can be readily related to the measured conductivity and shielding properties of the investigated materials. Filler segregation is well known to improve electrical and shielding properties [30–33]. However, multiple experimental steps are often required to obtain composites with aggregated fillers. In this work, aggregation of fillers leading to enhanced electromagnetic properties is readily obtained by adding stearic acid, which could be a cost-effective approach for industrial scale composite manufacturing.

Another effect of the addition of stearic acid is the lubrication of the particle/particle contacts. Comparing Fig. 9-a and Fig. 9-b, the presence of multiple small particles of several microns in diameter among dispersed particles of larger diameters can be observed in the composite free of stearic acid. The smaller particles might have been formed by erosion due to particle-particle contacts during mixing, since these small particles are much less present in the composite made using stearic acid. The lubrication effect of stearic acid is also evident in the torque measured during mixing (Figure S2, Supplementary Information Part), which was lower in the presence of stearic acid. Large torque variations suggesting erosion due to particle-particle contacts in the absence of stearic acid were no observed when stearic acid was added into the composite material [44,50].

The morphologies of the composites of PP/Ag-coated glass fibers prepared without and with stearic acid (at 3 vol%) are shown in Fig. 9-e and 9-f, for composite layers of 20 µm

thickness. The concentration of 3 vol% for the stearic acid was chosen because it leads to the highest increase in the electromagnetic shielding properties of our composite materials. A clear change in the composite morphology can be also observed with Ag-coated microfibers, well dispersed for composites free of stearic acid and aggregated in the presence of the stearic acid. The aggregates sizes of Ag-coated microfibers range from 100 to 300 µm with fibers-free polymer domains of equivalent sizes. The morphology difference is less striking than with the Tin particles but can be related as well to the improved electrical and shielding properties in the presence of stearic acid.

3.5 Proposed mechanism for the impact of stearic acid on composite morphology and properties

A mechanism to explain the impact of stearic acid on the morphology and the properties of the PP/Tin particles composites is presented in Fig. 10. During the composite processing, PP and stearic acid are introduced in the mixer first, at 190°C. Once they are molten and mixed, Tin microparticles are introduced in the mixing tank, too. In the first step (Figure 8), liquid drops of stearic acid (having a melting point of 69-70°C) and solid Tin particles are dispersed into the molten polymer matrix. Under mixing shear forces, the stearic acid comes in contact with Tin particles and reacts with their surface, forming a surface layer of Tin stearate. In the second step, the stearic acid being only partially miscible in the molten PP matrix [68] and with the presence of a bonded layer of fatty acid on the particles surface, stearic acid/Tin particles domains are formed. Then, mixing shear forces lead to the aggregation of these domains. Bigger domains are thus formed and stabilized by the surface bonds formed between the stearic acid and the Tin particles and by the immiscibility of stearic acid with the PP matrix. A consequence of this aggregation is the percolation of Tin particles. The next step is the improved electrical

percolation of these bigger stearic acid/Tin particles domains, resulting in enhanced composite conductivity and shielding properties. This mechanism will be demonstrated in the following sections of the current study, based on analysis by infrared spectroscopy, contact angle, interfacial tension and infrared transmission microscopy.

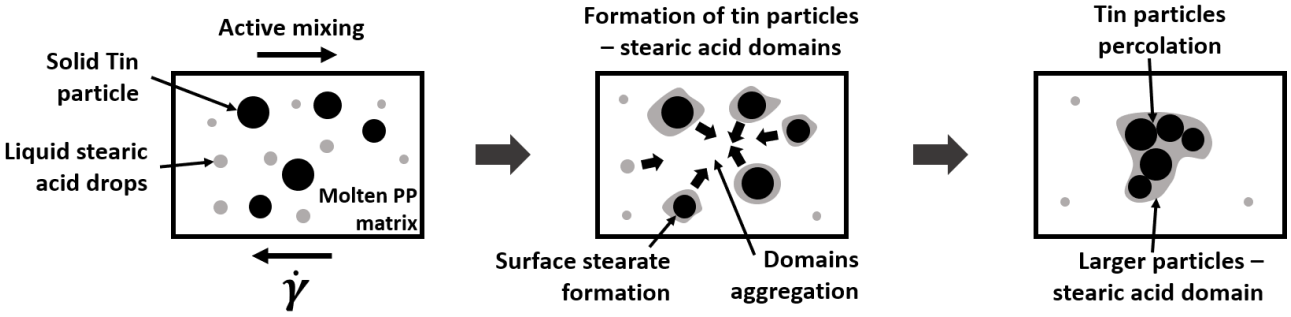

Fig. 10: *Proposed mechanism for the effect of stearic acid during mixing on the final composite morphology. First phase: solid Tin particles and liquid stearic drops are dispersed in the molten PP matrix. Second phase: stearic acid reacts with the surface of Tin particles and forms particle/stearic acid domains. Mixing shear forces drive the domains to aggregate. Surface forces stabilize the aggregates. Third phase: Bigger particles/stearic acid domains are formed and reunite several particles that percolate. The same driving forces then lead to the global percolation of bigger aggregates.*

The impact of aggregation on the electrical percolation is well-studied in the scientific literature, and various conclusions are reported. For instance, R. H. Schmidt et al. studied the effect of aggregation on the electrical conductivity of polymer/carbon nanotube composite films and found that aggregation causes a drop in conductivity at high nanotube loading [90]. F. Coupette et al. studied the percolation of rigid fractal carbon black aggregates and concluded that the concentration of large carbon black aggregates has a stronger influence on the percolation threshold than the concentration of small aggregates [91]. In another study [92], N.

Lebovka et al. reported a two-step percolation in aggregating systems. It has been also reported that functionalization of fillers leads to a gradual breakdown of nanorods aggregation [93]. However, the impact of aggregation on the EM shielding properties of composite materials is much less studied in the scientific literature.

3.6 Infrared spectroscopy of Tin particles and Silver-coated glass microfibers mixed with stearic acid

To investigate the reactivity of stearic acid with the metallic fillers used in the current study, the fatty acid was directly mixed with Tin particles and with Ag-coated glass microfibers at 100°C. The infrared spectra of pure Tin particles, pure Ag-coated glass microfibers, pure stearic acid and of 50/50 vol% blends of these compounds are displayed in Figure 11. For the stearic acid spectrum, the peaks observed at 2916 and 2850 cm^{-1} can be attributed to C-H single bond vibrations. The peaks at 1710, 1470 and 1300 cm^{-1} are attributed to C=O carboxyl double bond, CH_2 and CH_3 (rocking and bending modes), and C-O carboxyl single bond, respectively. A very wide, medium intensity absorption band between 2500 and 3500 cm^{-1} can be attributed to the acid O-H bond. Tin particles and Ag-coated glass microfibers show high absorbance in the whole spectral range. The presence of surface oxide O-H bonds is characterized by the presence of a wide, high intensity band between 3400 and 3600 cm^{-1}. This band results from the unsaturated bonds on the metal surface [69,70]. The infrared spectra of stearic acid blends with the two metallic fillers show the appearance of a novel peak at 1644 and 1637 cm^{-1} for Tin particles and Silver-coated glass fibers, respectively. These new peaks are due to the formation of a metal-stearate complex on the metallic surfaces. The reaction of stearic acid on mineral and metallic surfaces has been reported multiple times in the past [49,71,72], and the following chemical equation with metal atoms M can be proposed:

$$M - OH + CH_3(CH_2)_{16} - COOH \rightarrow M - OOC - CH_3(CH_2)_{16} + H_2O \quad (16)$$

A covalent bond is formed through the exchange of acid H^+ of the stearic acid, leading to the formation of a water molecule. The presence of the covalently bonded heavy metallic atoms shifts the absorption wavenumber of the nearby carboxyl double bond C=O, resulting in the apparition of new peaks. This chemical equation is a simplification of the chemical interaction between stearic acid and metallic surfaces. Lim et al. suggested, for instance, that the bond can be monodentate (one oxygen atom of the fatty acid carboxyl group interacts with one metal atom), bidentate (two oxygen atoms interact with the metal atom) or bridging (the two oxygen atoms interact with two different metal atoms) [72]. Thus, as the liquid stearic acid and the metallic fillers are mixed with the molten PP matrix, a covalently bonded layer of stearic acid forms on the metallic surfaces of the fillers.

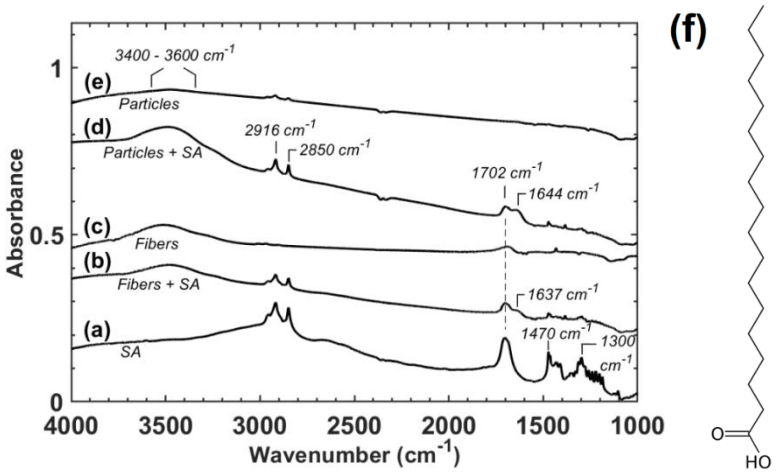

Fig. 11: *Transmission infrared spectroscopy spectra of Tin particles and Ag-coated glass microfibers and their blends with stearic acid. The blends are made at 100°C. (a) Pure stearic acid, (b) 50/50 vol% blend of microfibers with stearic acid, (c) pure microfibers, (d) 50/50 vol% blend of Tin particles with stearic acid and (e) pure Tin particles. (f) Stearic acid chemical structure.*

3.7 Modifications of surface properties of metallic fillers in the presence of stearic acid

To characterize the effect of stearic acid on the surface properties of metallic fillers, the water contact angle method was used on stearic acid/Tin particles blends and stearic acid/Ag-coated glass microfibers blends. The value of the water contact angle is related to the surface property of materials: the surface is hydrophilic if the angle is lower than 90° and hydrophobic if the angle is greater than 90°. The results are shown in Figure 12. The low angle values of pure Tin particles and pure Ag-coated glass fibers (39° and 18°, respectively) indicate the hydrophilic nature of the metallic surfaces due to the presence of metal oxide [73]. On contrary, the water contact angle of pure stearic acid is equal to 101°, corresponding to the hydrophobic nature of the fatty acid. All the blends display hydrophobic contact angle values, even at low concentrations of stearic acid. Thus, the effect of stearic acid on the surface properties of metallic fillers is radical, changing their hydrophilic nature into a hydrophobic one. The water contact angles values higher than the contact angle of pure stearic acid – in particular for the microfibers – is due to the surface roughness that is known to increase the apparent water contact angle [74].

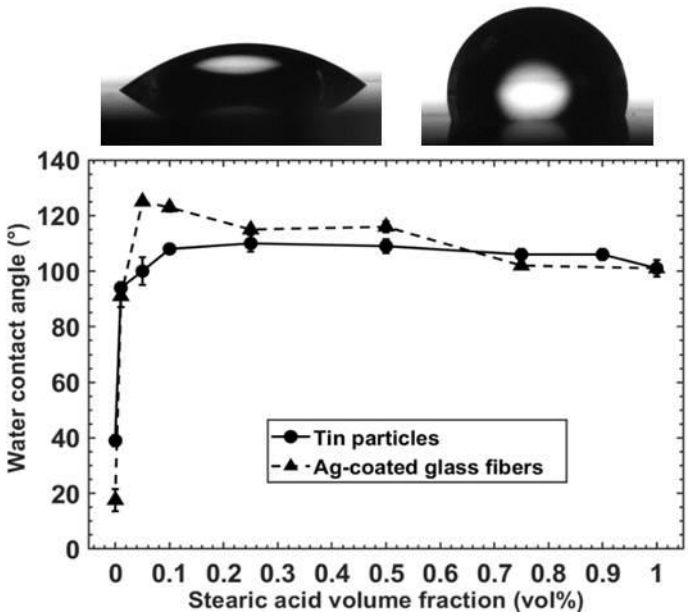

Fig. 12: *Water droplet contact angle on blends of Tin particles and Ag-coated glass microfibers with stearic acid as a function of the concentration of stearic acid. Mixing was made at 100°C. Images of the water droplet for pure Tin particles (left) and pure stearic acid (right) are shown.*

Since surface properties of fillers are converging to the ones of the pure stearic acid even at low fatty acid concentrations, this indicates that stearic acid rapidly covers the fillers surface entirely. The fatty acid concentration to achieve a monolayer covering the entire surface of fillers can be calculated using the following formula [49]:

$$\boldsymbol{c_{SA} = e \times SSA \times \rho_{SA}} \quad (17)$$

Where the weight concentration of adsorbed stearic acid is c_{SA}, the thickness of the absorbed layer is e, the specific surface area of the fillers is SSA. The latter can be estimated to 18 m^2/kg for Tin particles and 95 m^2/kg for Ag-coated glass fibers, by taking into account the geometrical dimensions of these fillers. ρ_{SA} is the density of the stearic acid. The length of a carbon-carbon single bond is approximately 1.54 angstrom. This allows one to calculate the approximate length of the stearic acid molecule (Fig. 11-f). A value of 2.2 nm is obtained, by taking into consideration the bent atomic bonds (109.54°) and the carboxyl head. Hence, the

calculation of the concentration of absorbed stearic acid for a monolayer leads to a relative weight concentration of 0.0037 wt% for Tin-particles and 0.020 wt% for Ag-coated glass microfibers. These values can be converted to volume concentrations, leading to 0.03 vol% for Tin-Particles and 0.06 vol% for Ag-coated microfibers. The obtained values are in agreement with our experimental results since the water contact angle starts to change at 0.01 vol% stearic acid and reaches the fatty acid value for 0.05 vol%.

3.8 Interfacial tension analysis of tertiary PP/metallic filler/stearic acid blends

The interfacial tension between two liquids or a solid and a liquid characterizes the affinity between the two compounds and their ability to mix and interact with each other. From values of the surface tension, the interfacial tension can be estimated theoretically using the Owens, Wendt and Wu equations [75,76]:

$$\boldsymbol{\gamma_{12} = \gamma_1 + \gamma_2 - \frac{4.\gamma_1^d.\gamma_2^d}{\gamma_1^d+\gamma_2^d} - \frac{4.\gamma_1^p.\gamma_2^p}{\gamma_1^p+\gamma_2^p}} \quad (18)$$

$$\boldsymbol{\gamma_{12} = \gamma_1 + \gamma_2 - 2.\sqrt{\gamma_1^d.\gamma_2^d} - \frac{4.\gamma_1^p.\gamma_2^p}{\gamma_1^p+\gamma_2^p}} \quad (19)$$

where γ_{12} is the interfacial tension between compound 1 and 2, and γ_1 and γ_2 are the surface tensions of compound 1 and 2, respectively. Exponents *d* and *p* indicates the dispersive or polar component of the surface tension. Eq. 18 is the harmonic-mean equation suitable for interfaces between organic liquids and organic polymers, and Eq. 19 is the geometric-harmonic-mean equation suitable for the interface between high- and low-energy phases such as metals and organic polymers [76]. Elias et al. reported the surface tension of PP 7060 and its temperature dependence using the Guggenheim relation [77,78]. At 190°C, the surface tension of this

polymer in the molten state is 20 mN/m, without the polar component. At the same temperature, the surface tension of the liquid stearic acid is 19.2 mN/m. As reported in the literature, the polar component can be considered negligible [45,79,80]. Using Eq. 18, a theoretical prediction of the interfacial tension between PP 7060 and stearic acid at 190°C gives the value of 0.02 mN/m. These two compounds have thus a good affinity at the mixing temperature, explaining the easy dispersion of stearic acid drops in the molten polymer and the stabilization of Tin particles/stearic acid domains in the polymer matrix.

To take into account the interaction between the stearic acid and the surface of the metallic fillers, we note that pure metals usually exhibit high values of surface tension, such as 570 mN/m for pure Tin at 190°C [81]. However, with the oxidation of the metallic surfaces, surface tensions have been reported to considerably decrease [82–84], leading to a more favorable affinity of the metallic fillers with the stearic acid. This effect is also coherent with the low water contact angle values of Tin particles and Ag-coated glass fibers. The actual surface tension values at room temperature seem thus to be close to the one of water (73 mN/m). Hence, stearic acid can wet the metallic surface of the fillers and then form a covalently bonded layer of fatty acid on the whole metallic surface. The consequence is the increased affinity between the metallic surfaces covered with bonded stearic acid and the other (non-bonded) fatty acid molecules present in the blends. This favors the formation of metallic fillers/liquid stearic acid domains. The low PP/stearic acid interfacial tension results in the good compatibility of the molten polymer with these domains, preventing the phenomena of complete phase demixing.

3.9 Infrared transmission microscopy

Composite layers of 20 µm-thickness prepared by microtoming were analyzed using an infrared transmission microscope. In the case of PP/Tin particles/stearic acid composites, the areas with a high concentration of particles (particles domains) are well separated from the areas with no particles (polymer domains). This enables one to measure the infrared spectra of these different domains with a 20x20 µm² surface infrared beam and investigate local variations in the concentration of stearic acid (Fig. 10). The measured zones and the resulting spectra are displayed in Fig. 13-a and 13-b, respectively, for composites of PP/15 vol% Tin particles without and with the addition of stearic acid (6 vol%). Intense peaks related to PP are visible in all spectra in the 1300-1500 cm^{-1} and 2800-3000 cm^{-1} zones. The two absorption peaks centered on 2350 cm^{-1} are due to carbon dioxide which could not be completely eliminated. For the composites free of stearic acid, the polymer domain spectra were measured in areas with fewer Tin particles.

The absorption in the particle domains is higher than the absorption corresponding to polymer domains, because of the higher absorbance of particles, as noted in the previous infrared measurements (Fig. 11). The absorption peak at 1710 cm^{-1} (carboxyl C=O double bond), characteristic to stearic acid, is only visible for composites prepared using the stearic acid. Metal stearate absorption peaks are not visible because of their too low concentration. Stearic acid is present in both polymer and particles domains.

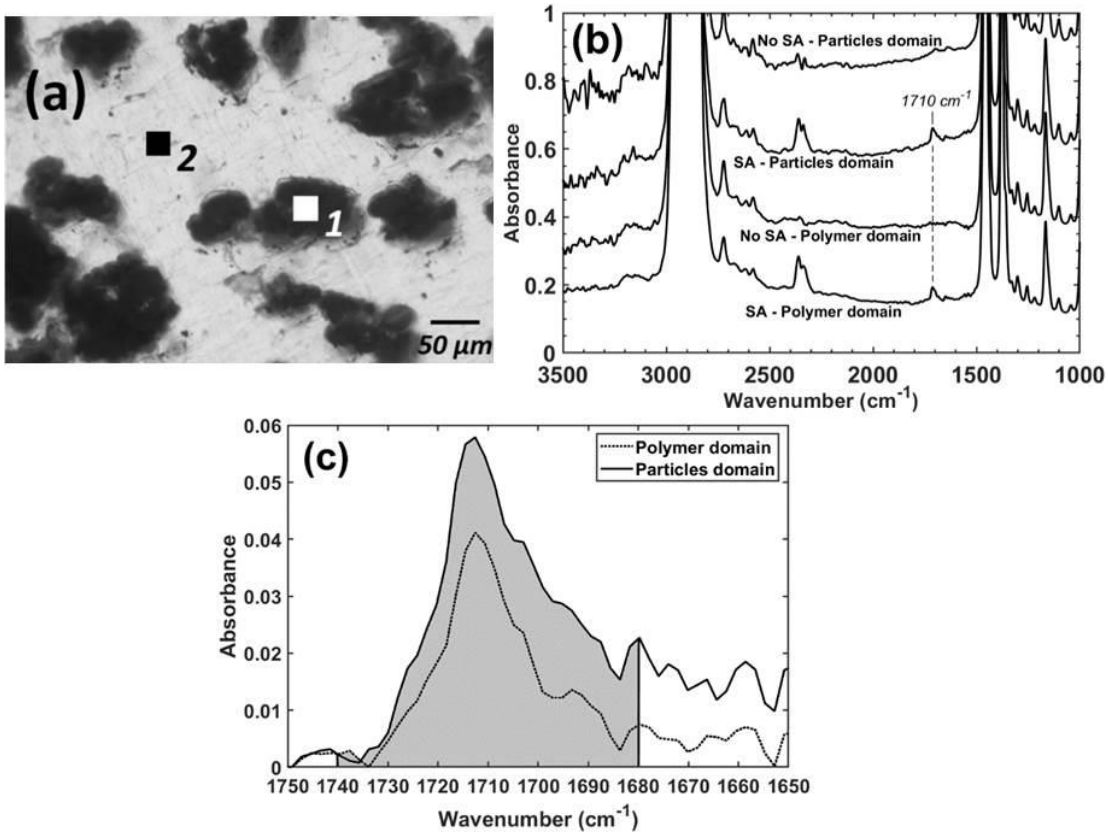

Fig. 13: *Transmission infrared microscopy of PP/Tin particles composites with and without stearic acid. (a) Optical microscopy image of PP/15 vol% Tin particles/6 vol% stearic acid. The squares indicate the measurement zones (20x20 µm²) of the infrared measurement: the white square (1) is the measurement of a Tin particle domain and the black square (2) is the measurement of a polymer matrix domain. (b) Infrared spectra of the investigated domains corresponding to PP/15 vol% Tin particles without and with 6 vol% stearic acid. (c) Close-up on the peak attributed to the stearic acid and comparison between polymer and particles domains for the composite containing stearic acid. Grey area with a baseline correction is used to compare the stearic acid content between the two different domains. Results are listed in Table 5.*

To investigate the variations of concentration between the two domain types, the spectral area under the absorbance curves around the stearic acid peak was measured using a baseline correction (Fig. 13-c). The results are listed in Table 5. For Tin particles composites

with 1 and 6 vol% stearic acid, and Ag-coated glass fibers with 2 vol% stearic acid, the area under the absorbance curve around the peak corresponding to the stearic acid is larger in the filler domains, with a significant relative variation by 39% to 86%. Absorbance is related to the concentration of the absorbing groups, exhibiting a linear dependence expressed by the Beer-Lambert law. Hence, the concentration of stearic acid is higher in filler domains compared to polymer domains by about 39% to 86%, giving a strong support to our proposed mechanism (Fig. 10). For the fibers-based composite with 4 vol% stearic acid, no difference in the stearic acid concentration was observed between the two domain types. This can be related to the reduced conductivity and shielding properties of this composite compared to the composites prepared with lower stearic acid concentrations. The stearic acid excess does not interact with the fibers and is homogeneously dispersed in the composite, which explains the infrared results as well as the lower mixing shear related to a poor filler dispersion and degraded physical properties.

Table 5: *Spectral area of filler domains and polymer domains, as described in Figure 11. The excess in filler domain is the ratio of the filler domain spectral area over the area of the polymer domain, expressed in percentage.*

	Filler volume fraction (vol%)	**Stearic acid volume fraction (vol%)**	**Filler domain spectral area (cm^{-1})**	**Polymer domain spectral area (cm^{-1})**	**Excess in filler domain**
Tin particles composite 1	15	1	1,4 ± 0,2	0,8 ± 0,1	+ 86 %

Tin particles composite 2	15	6	3,6 ± 0,2	2,6 ± 0,2	+ 39 %
Fibers composite 1	10	2	6,0 ± 0,8	3,8 ± 0,5	+ 56 %
Fibers composite 2	10	4	8,4 ± 1,0	8,7 ± 1,3	- 4 %

An experiment showing the favored interactions of stearic acid with the Tin particles was also carried out. A delayed introduction of stearic acid into the pure PP matrix showed poor mixing between the PP matrix and the stearic acid with a lower mixing torque but not in the presence of metallic particles that tend to keep the fatty acid in the blend. Results are presented in Figure S4 in the Supplementary Information Part. The use of a different method for filler treatment by stearic acid [85] or the use of other thermoplastic resins and of a stearic acid analogous molecule [86,87] (ethylene bis(stearamide)) showed no significant differences in the shielding properties. Results are presented in Figures S5 and S6 in the Supplementary Information Part. This highlights the universal character of the proposed mechanism describing the impact of fatty acids or other analogous molecules on the morphology and shielding properties of composites filled with metallic fillers.

4. Conclusions

Polypropylene-based conductive composite materials have been prepared by melt mixing using two types of metallic fillers (hybrid Silver-coated glass microfibers and Tin microparticles). Their shielding properties have been investigated between 0.1 MHz and 18 GHz using two different experimental technique: coaxial cell method and waveguide method.

A guided electrical percolation taking place in the presence of steric acid leads to a substantial enhancement in the shielding effectiveness by more than 60 dB. This phenomenon corresponds to a drastic change in the composite morphology from a homogeneous to a heterogeneous distribution, leading unexpectedly to much higher conductivity values and substantially lower percolation thresholds (decreasing from 14.7 vol% to 6.9 vol% for Tin microparticles and from 3.95 vol% to 2.9 vol% for Ag-coated glass microfibers). The optimal stearic acid concentration for a maximum shielding effectiveness was determined for both types of composite materials. Materials with shielding effectiveness values as high as 90 dB for Tin microparticles and 91 dB for Ag-coated glass microfibers are obtained. The origin of this enhancement effect, driven by the interfacial interactions between the polymer, the metallic fillers and the steric acid, was investigated by using Infrared-Spectroscopy, contact angle measurements, interfacial tension analysis and optical microscopy. It is proven that much more efficient electrical percolation guided by a drastic reorganization of the composite morphology originates from a shear-induced coalescence of steric acid. Guiding the electrical percolation of metallic fillers represents thus a very efficient approach to greatly enhance the electromagnetic shielding properties of functional composite materials.

5. Acknowledgements

The financial support given by ANRT France through a CIFRE project is highly acknowledged. The authors would like to kindly acknowledge the help of Laurent Cavetier in fabricating some additional metallic elements necessary for the measurement cells.

References

[1] Thomassin, J.-M., C. Jérôme, T. Pardoen, C. Bailly, I. Huynen and C. Detrembleur. "Polymer/carbon based composites as electromagnetic interference (EMI) shielding materials," Materials Science and Engineering: R: Reports 74, 211–232 (2013).

[2] Wanasinghe, D., F. Aslani, G. Ma and D. Habibi. "Review of Polymer Composites with Diverse Nanofillers for Electromagnetic Interference Shielding," Nanomaterials 10, 541 (2020).

[3] Wanasinghe, D. and F. Aslani. "A review on recent advancement of electromagnetic interference shielding novel metallic materials and processes," Composites Part B: Engineering 176, 107207 (2019).

[4] Sankaran, S., K. Deshmukh, M. Basheer Ahamed and S. K. Khadheer Pasha. "Recent advances in electromagnetic interference shielding properties of metal and carbon filler reinforced flexible polymer composites: A review," Composites Part A 114, 49–71 (2018).

[5] Schultz, R. B., V. C. Plantz and D. R. Brush. "Shielding theory and practice," IEEE Transactions on electromagnetic compatibility 30, 187–201 (1988).

[6] Sudha, J. D., S. Sivakala, K. Patel and P. Radhakrishnan Nair. "Development of electromagnetic shielding materials from the conductive blends of polystyrene polyaniline-clay nanocomposite," Composites Part A: Applied Science and Manufacturing 41, 1647–1652 (2010).

[7] Zhenwei Liu, Fangwei Ling, Xingyuan Diao, Meirui Fu, Hongwei Bai, Qin Zhang, Qiang Fu. Stereocomplex-type polylactide with remarkably enhanced melt-processability and electrical performance via incorporating multifunctional carbon black. Polymer 188, 122136 (2020).

[8] Zhou, H., Z. Xiao, Y. Wang, X. Hao, Y. Xie, Y. Song, F. Wang and Q. Wang. "Conductive and fire-retardant wood/polyethylene composites based on a continuous honeycomb-like nanoscale carbon black network," Construction and Building Materials 233, 117369 (2020).

[9] Ryu, S. C., J. Y. Kim, C. Cho and W. N. Kim. "Improvements of the Electrical Conductivity and EMI Shielding Efficiency for the Polycarbonate/ABS/Carbon Fiber Composites Prepared by Pultrusion Process," Macromol. Res. 28, 118–125 (2020).

[10] Jiji Abraham, Mohammed Arif P, Priti Xavier, Suryasarathi Bose, Soney C. George; Nandakumar Kalarikkal, Sabu Thomas. Investigation into dielectric behaviour and electromagnetic interference shielding effectiveness of conducting styrene butadiene rubber composites containing ionic liquid modified MWCNT. Polymer 112, 102-115 (2017).

[11] Ji-un Jang, Ji Eun Cha, Seung Hwan Lee, Jaewoo Kim, Beomjoo Yang, Seong Yun Kim, Seong Hun Kim. Enhanced electrical and electromagnetic interference shielding properties of uniformly dispersed carbon nanotubes filled composite films via solvent-free process using ring-opening polymerization of cyclic butylene terephthalate. Polymer 186, 122030 (2020).

[12] Lecocq, H., N. Garois, O. Lhost, P.-F. Girard, P. Cassagnau and A. Serghei. "Polypropylene/carbon nanotubes composite materials with enhanced electromagnetic interference shielding performance: Properties and modeling," Composites Part B: Engineering 189, 107866 (2020).

[13] Shuai Zhang, Shuya Yin, Qichao Ran, Qiang Fu, Yi Gu. Facile preparation of polybenzoxazine/graphene nanocomposites for electromagnetic interference shielding. Polymer 162, 20-28 (2019).

[14] Liang, C., P. Song, H. Qiu, Y. Huangfu, Y. Lu, L. Wang, J. Kong and J. Gu. "Superior electromagnetic interference shielding performances of epoxy composites by introducing

highly aligned reduced graphene oxide films," Composites Part A: Applied Science and Manufacturing 124, 105512 (2019).

[15] Ameli, A., M. Nofar, S. Wang and C. B. Park. "Lightweight Polypropylene/Stainless-Steel Fiber Composite Foams with Low Percolation for Efficient Electromagnetic Interference Shielding," ACS Appl. Mater. Interfaces 6, 11091–11100 (2014).

[16] Dravid, S. V., S. D. Bhosale, S. Datar and R. K. Goyal. "Nickel Nanoparticle-Filled High-Performance Polymeric Nanocomposites for EMI Shielding Applications," Journal of Elec Materi 49, 1630–1637 (2020).

[17] Duan, H., Y. Xu, D.-X. Yan, Y. Yang, G. Zhao and Y. Liu. "Ultrahigh molecular weight polyethylene composites with segregated nickel conductive network for highly efficient electromagnetic interference shielding," Materials Letters 209, 353–356 (2017).

[18] Gargama, H., A. K. Thakur and S. K. Chaturvedi. "Polyvinylidene fluoride/nanocrystalline iron composite materials for EMI shielding and absorption applications," Journal of Alloys and Compounds 654, 209–215 (2016).

[19] Al-Saleh, M. H., G. A. Gelves and U. Sundararaj. "Copper nanowire/polystyrene nanocomposites: Lower percolation threshold and higher EMI shielding," Composites Part A: Applied Science and Manufacturing 42, 92–97 (2011).

[20] Ravindren, R., S. Mondal, K. Nath and N. C. Das. "Prediction of electrical conductivity, double percolation limit and electromagnetic interference shielding effectiveness of copper nanowire filled flexible polymer blend nanocomposites," Composites Part B: Engineering 164, 559–569 (2019).

[21] Gao, Y.-N., Y. Wang, T.-N. Yue, Y.-X. Weng and M. Wang. "Multifunctional cotton non-woven fabrics coated with silver nanoparticles and polymers for antibacterial, superhydrophobic and high performance microwave shielding," Journal of Colloid and Interface Science 582, 112–123 (2021).

[22] Wang, Z., J. Ren, R. Liu, X. Sun, D. Huang, W. Xu, J. Jiang, K. Ma and Y. Liu. “Three dimensional core-shell structured liquid metal/elastomer composite via coaxial direct ink writing for electromagnetic interference shielding,” Composites Part A: Applied Science and Manufacturing 136, 105957 (2020).

[23] Renhui Sun, Hao-Bin Zhang, Ji Liu, Xi Xie, Rui Yang, Yue Li, Song Hong, Zhong-Zhen Yu. Highly Conductive Transition Metal Carbide/Carbonitride(MXene)@polystyrene Nanocomposites Fabricated by Electrostatic Assembly for Highly Efficient Electromagnetic Interference Shielding, Advanced Functional Materials. 27, 1702807 (2017).

[24] Jia-Qi Luo, Sai Zhao, Hao-Bin Zhang, Zhiming Deng, Lulu Li, Zhong-Zhen Yu, Flexible, stretchable and electrically conductive MXene/natural rubber nanocomposite films for efficient electromagnetic interference shielding. Composites Science and Technology 182, 107754 (2019).

[25] Ming-Ke Xu, Ji Liu, Hao-Bin Zhang, Yu Zhang, Xinyu Wu, Zhiming Deng, and Zhong-Zhen Yu. Electrically Conductive Ti3C2Tx MXene/Polypropylene Nanocomposites with an Ultralow Percolation Threshold for Efficient Electromagnetic Interference Shielding. Journal of Industrial and Engineering Chemistry Research 60, 4342-4350 (2021)

[26] Sun, X., X. Liu, X. Shen, Y. Wu, Z. Wang and J.-K. Kim. “Graphene foam/carbon nanotube/poly(dimethyl siloxane) composites for exceptional microwave shielding,” Composites Part A: Applied Science and Manufacturing 85, 199–206 (2016).

[27] Lalan, V. and S. Ganesanpotti. “Broadband Electromagnetic Response and Enhanced Microwave Absorption in Carbon Black and Magnetic Fe3O4 Nanoparticles Reinforced Polyvinylidenefluoride Composites,” Journal of Elec Materi 49, 1666–1676 (2020).

[28] Ju, J., T. Kuang, X. Ke, M. Zeng, Z. Chen, S. Zhang and X. Peng. “Lightweight multifunctional polypropylene/carbon nanotubes/carbon black nanocomposite foams with

segregated structure, ultralow percolation threshold and enhanced electromagnetic interference shielding performance," Composites Science and Technology 193, 108116 (2020).

[29] Raagulan, K., R. Braveenth, L. Ro Lee, J. Lee, B. Kim, J. Moon, S. Lee and K. Chai. "Fabrication of Flexible, Lightweight, Magnetic Mushroom Gills and Coral-Like MXene–Carbon Nanotube Nanocomposites for EMI Shielding Application," Nanomaterials 9, 519 (2019).

[30] Wang, H., K. Zheng, X. Zhang, T. Du, C. Xiao, X. Ding, C. Bao, L. Chen and X. Tian. "Segregated poly(vinylidene fluoride)/MWCNTs composites for high-performance electromagnetic interference shielding," Composites Part A: Applied Science and Manufacturing 90, 606–613 (2016).

[31] Yuan, D., H. Guo, K. Ke and I. Manas-Zloczower. "Recyclable conductive epoxy composites with segregated filler network structure for EMI shielding and strain sensing," Composites Part A: Applied Science and Manufacturing 132, 105837 (2020).

[32] Zhang, Y.-P., C.-G. Zhou, W.-J. Sun, T. Wang, L.-C. Jia, D.-X. Yan and Z.-M. Li. "Injection molding of segregated carbon nanotube/polypropylene composite with enhanced electromagnetic interference shielding and mechanical performance," Composites Science and Technology 197, 108253 (2020).

[33] Ren, F., Z. Li, L. Xu, Z. Sun, P. Ren, D. Yan and Z. Li. "Large-scale preparation of segregated PLA/carbon nanotube composite with high efficient electromagnetic interference shielding and favourable mechanical properties," Composites Part B: Engineering 155, 405–413 (2018).

[34] Zhao, Y. et al. "Facile preparation of lightweight PE/PVDF/Fe3O4/CNTs nanocomposite foams with high conductivity for efficient electromagnetic interference shielding," Composites Part A: Applied Science and Manufacturing 139, 106095 (2020).

[35] Yang, Z., Y. Zhang and B. Wen. “Enhanced electromagnetic interference shielding capability in bamboo fiber@polyaniline composites through microwave reflection cavity design,” Composites Science and Technology 178, 41–49 (2019).

[36] Ghosh, S., S. Ganguly, P. Das, T. K. Das, M. Bose, N. K. Singha, A. K. Das and N. Ch. Das. “Fabrication of Reduced Graphene Oxide/Silver Nanoparticles Decorated Conductive Cotton Fabric for High Performing Electromagnetic Interference Shielding and Antibacterial Application,” Fibers Polym 20, 1161–1171 (2019).

[37] Wang, R., H. Yang, J. Wang and F. Li. “The electromagnetic interference shielding of silicone rubber filled with nickel coated carbon fiber,” Polymer Testing 38, 53–56 (2014).

[38] Buch, A. “Pure metals properties: A scientific and technical handbook” (1999).

[39] Zeng, Z., W. Li, N. Wu, S. Zhao and X. Lu. “Polymer-Assisted Fabrication of Silver Nanowire Cellular Monoliths: Toward Hydrophobic and Ultraflexible High-Performance Electromagnetic Interference Shielding Materials,” ACS Appl. Mater. Interfaces 12, 38584–38592 (2020).

[40] Tan, Y.-J., J. Li, Y. Gao, J. Li, S. Guo and M. Wang. “A facile approach to fabricating silver-coated cotton fiber non-woven fabrics for ultrahigh electromagnetic interference shielding,” Applied Surface Science 458, 236–244 (2018).

[41] Olivero, D. A. and D. W. Radford. “A multiple percolation approch to EMI shielding composites incorporating conductive filles,” Journal of Reinforced Plastics and Composites 17, 674–690 (1998).

[42] Zhang, K., H.-O. Yu, K.-X. Yu, Y. Gao, M. Wang, J. Li and S. Guo. “A facile approach to constructing efficiently segregated conductive networks in poly(lactic acid)/silver nanocomposites via silver plating on microfibers for electromagnetic interference shielding,” Composites Science and Technology 156, 136–143 (2018).

[43] Hatzikiriakos, S. G., I. B. Kazatchkov and D. Vlassopoulos. “Interfacial phenomena in the capillary extrusion of metallocene polyethylenes,” Journal of Rheology 41, 1299–1316 (1997).

[44] Fisch, M. and R. Bacaloglu. “Study of additive compatibility with poly(vinyl chloride) (PVC). 2: Dynamic mechanical analysis of PVC lubrication by stearic acid and its derivatives,” J Vinyl Addit Technol 4, 4–11 (1998).

[45] Anneken, D. J., S. Both, R. Christoph, G. Fieg, U. Steinberner and A. Westfechtel. “Fatty Acids,” in Ullmann’s Encyclopedia of Industrial Chemistry (ed. Wiley-VCH Verlag GmbH & Co. KGaA) a10_245.pub2 (Wiley-VCH Verlag GmbH & Co. KGaA, 2006). doi:10.1002/14356007.a10_245.pub2.

[46] Nhan, H. N., M. Jean-Louis and W. Jean-Luc. “Modeling of Electromagnetic Shielding Effectiveness of Multilayer Conducting Composites in the Microwave Band,” in 2006 First International Conference on Communications and Electronics 482–485 (IEEE, 2006). doi:10.1109/CCE.2006.350874.

[47] Sun, J., W. Wang and Q. Yue. “Review on Microwave-Matter Interaction Fundamentals and Efficient Microwave-Associated Heating Strategies,” Materials 9, 231 (2016).

[48] Kirkpatrick, S. “Percolation and Conduction,” Rev. Mod. Phys. 45, 574–588 (1973).

[49] Auscher, M. C., R. Fulchiron, N. Fougerouse, T. Périé and P. Cassagnau. “Zirconia based feedstocks: Influence of particle surface modification on the rheological properties,” Ceramics International 43, 16950–16956 (2017).

[50] Osman, M. A., A. Atallah, T. Schweizer and H. C. Öttinger. “Particle–particle and particle-matrix interactions in calcite filled high-density polyethylene—steady shear,” Journal of Rheology 48, 1167–1184 (2004).

[51] Patti, A., H. Lecocq, A. Serghei, D. Acierno and P. Cassagnau. “The universal usefulness of stearic acid as surface modifier: applications to the polymer formulations and composite processing,” Journal of Industrial and Engineering Chemistry 96, 1–33 (2021).

[52] Wei, B., L. zhang and S. Yang. “Polymer composites with expanded graphite network with superior thermal conductivity and electromagnetic interference shielding performance,” Chemical Engineering Journal 404, 126437 (2021).

[53] Iqbal, M. Z., G. M. Mamoor, T. Bashir, M. S. Irfan and M. B. Manzoor. “A study on polystyrene - metal powder conductive composites,” Journal of Chemical Engineering 25, 4 (2010).

[54] Nguyen, D. M., T. N. Vu, T. M. L. Nguyen, T. D. Nguyen, C. N. H. Thuc, Q. B. Bui, J. Colin and P. Perré. “Synergistic Influences of Stearic Acid Coating and Recycled PET Microfibers on the Enhanced Properties of Composite Materials,” Materials 13, 1461 (2020).

[55] Yi, Z., J. Yang, X. Liu, L. Mao, L. Cui and Y. Liu. “Enhanced mechanical properties of poly(lactic acid) composites with ultrathin nanosheets of MXene modified by stearic acid,” J Appl Polym Sci 137, 48621 (2020).

[56] Xiong, C., Z. Zhou, W. Xu, H. Hu, Y. Zhang and L. Dong. “Polyurethane/carbon black composites with high positive temperature coefficient and low critical transformation temperature,” Carbon 43, 1788–1792 (2005).

[57] Vanga-Bouanga, C., T. F. Heid, M. F. Frechette and E. David. “Influence of interface on the dielectric response, electrical and thermal conductivity of high density polyethylene based composites,” in 2015 IEEE Conference on Electrical Insulation and Dielectric Phenomena (CEIDP) 709–712 (IEEE, 2015). doi:10.1109/CEIDP.2015.7352138.

[58] Yu, C., Y. S. Kim, D. Kim and J. C. Grunlan. “Thermoelectric Behavior of Segregated-Network Polymer Nanocomposites,” Nano Lett. 8, 4428–4432 (2008).

[59] Lee, S. H., S. Yu, F. Shahzad, J. P. Hong, W. N. Kim, C. Park, S. M. Hong and C. M. Koo. “Highly anisotropic Cu oblate ellipsoids incorporated polymer composites with excellent performance for broadband electromagnetic interference shielding,” Composites Science and Technology 144, 57–62 (2017).

[60] Jung, J., H. Lee, I. Ha, H. Cho, K. K. Kim, J. Kwon, P. Won, S. Hong and S. H. Ko. “Highly Stretchable and Transparent Electromagnetic Interference Shielding Film Based on Silver Nanowire Percolation Network for Wearable Electronics Applications,” ACS Appl. Mater. Interfaces 9, 44609–44616 (2017).

[61] Oh, H.-J., V.-D. Dao and H.-S. Choi. “Electromagnetic shielding effectiveness of a thin silver layer deposited onto PET film via atmospheric pressure plasma reduction,” Applied Surface Science 435, 7–15 (2018).

[62] Xu, Z. and H. Hao. “Electromagnetic interference shielding effectiveness of aluminum foams with different porosity,” Journal of Alloys and Compounds 617, 207–213 (2014).

[63] Lu, Y., Q. Liang and W. Li. “Fabrication of copper/modal fabric composites through electroless plating process for electromagnetic interference shielding,” Materials Chemistry and Physics 140, 553–558 (2013).

[64] Lu, Y., Q. Liang and L. Xue. “Electroless nickel deposition on silane modified bamboo fabric through silver, copper or nickel activation,” Surface and Coatings Technology 206, 3639–3644 (2012).

[65] Dou, Z., G. Wu, X. Huang, D. Sun and L. Jiang. “Electromagnetic shielding effectiveness of aluminum alloy–fly ash composites,” Composites Part A: Applied Science and Manufacturing 38, 186–191 (2007).

[66] Wu, G., X. Huang, Z. Dou, S. Chen and L. Jiang. “Electromagnetic interfering shielding of aluminum alloy–cenospheres composite,” J Mater Sci 42, 2633–2636 (2007).

[67] Li, Y., J. Liu, S. Wang, L. Zhang and B. Shen. “Self-templating graphene network composites by flame carbonization for excellent electromagnetic interference shielding,” Composites Part B: Engineering 182, 107615 (2020).

[68] Broda, J., C. Slusarczyk, J. Fabia and A. Demsar. “Formation and properties of polypropylene/stearic acid composite fibers,” Textile Research Journal 86, 64–71 (2016).

[69] Socrates, G. “Infrared and Raman Characteristic Group Frequencies: Tables and Charts” (John Wiley & Sons, 2004).

[70] Lin, C., B. Wang, Y. Cheng and C. Wang. “Influence of stearic acid on the structure and rheological behavior of injection-molded ZTA suspensions,” Mater Sci-Pol 31, 36–42 (2013).

[71] Dong, Z., Y. Wan, S. Yang, C. Qi and J. Zhang. “Enhanced wear resistance of sol–gel TiO2 film on a carbon steel in unlubricated sliding against steel ball by stearic acid modification,” J Sol-Gel Sci Technol 66, 460–465 (2013).

[72] Lim, M. S. et al. “Adsorption and Desorption of Stearic Acid Self-Assembled Monolayers on Aluminum Oxide,” Langmuir 23, 2444–2452 (2007).

[73] Kenney, J. T., W. P. Townsend and J. A. Emerson. “Tin and iron hydrous oxide deposits on polyethylene, teflon, and paraffin,” Journal of Colloid and Interface Science 42, 589–596 (1973).

[74] Wenzel, R. N. “Resistance of solid surfaces to wetting by water,” Ind. Eng. Chem. 28, 988–994 (1936).

[75] Owens, D. K. and R. C. Wendt. “Estimation of the surface free energy of polymers,” J. Appl. Polym. Sci. 13, 1741–1747 (1969).

[76] Wu, S. “Interfacial and Surface Tensions of Polymers,” Journal of Macromolecular Science, Part C: Polymer Reviews 10, 1–73 (1974).

[77] Elias, L., F. Fenouillot, J. C. Majeste and Ph. Cassagnau. “Morphology and rheology of immiscible polymer blends filled with silica nanoparticles,” Polymer 48, 6029–6040 (2007).

[78] Guggenheim, E. A. “The Principle of Corresponding States,” The Journal of Chemical Physics 13, 253–261 (1945).

[79] Zdziennicka, A., K. Szymczyk, B. Jańczuk, R. Longwic and P. Sander. “Surface, Volumetric, and Wetting Properties of Oleic, Linoleic, and Linolenic Acids with Regards to Application of Canola Oil in Diesel Engines,” Applied Sciences 9, 3445 (2019).

[80] Ferfis, J. L. “The wettability of cellulose film as affected by vapor-phase adsorption of amphipathic molecules,” (Lawrence University, 1974).

[81] Gancarz, T., Z. Moser, W. Gąsior, J. Pstruś and H. Henein. “A Comparison of Surface Tension, Viscosity, and Density of Sn and Sn–Ag Alloys Using Different Measurement Techniques,” Int J Thermophys 32, 1210–1233 (2011).

[82] Fiori, L., E. Ricci and E. Arato. “Dynamic surface tension measurements on molten metal-oxygen systems: model validation on molten tin,” Acta Materialia 51, 2873–2890 (2003).

[83] Lee, J., T. Tanaka, M. Yamamoto and S. Hara. “Effect of Oxygen on Surface Tension of Liquid Ag-Sn Alloys,” Mater. Trans. 45, 625–629 (2004).

[84] Khan, M. R., C. B. Eaker, E. F. Bowden and M. D. Dickey. “Giant and switchable surface activity of liquid metal via surface oxidation,” Proc Natl Acad Sci USA 111, 14047–14051 (2014).

[85] Hernández, Y. et al. “Stearic acid as interface modifier and lubricant agent of the system: Polypropylene/calcium carbonate nanoparticles,” Polym Eng Sci 59, E279–E285 (2019).

[86] Nouri, A., P. D. Hodgson and C. Wen. “Study on the Role of Stearic Acid and Ethylene-bis-stearamide on the Mechanical Alloying of a Biomedical Titanium Based Alloy,” Metall and Mat Trans A 41, 1409–1420 (2010).

[87] Pluta, M., J. Bojda, E. Piorkowska, M. Murariu, L. Bonnaud and P. Dubois. “The effect of halloysite nanotubes and N,N’- ethylenebis (stearamide) on the properties of polylactide nanocomposites with amorphous matrix,” Polymer Testing 61, 35–45 (2017).

[88] Patti A., Acierno D., Lecocq H., Serghei A., Cassagnau P. Viscoelastic behaviour of highly filled polypropylene with solid and liquid Tin microparticles: influence of the stearic acid additive, Rheologica Acta 60, 661–673 (2021).

[89] Jesús Esteban, Serafim Bakalis, Claire Duckitt, Hossam Tantawy, Peter J. Fryer. On the Discrimination of Models for the Viscometric Properties of Myristic, Palmitic and Stearic Acids and Their Binary Mixtures. Eur. J. Lipid. Sci. Technol. 120, 1700279 (2018).

[90] Ronald H. Schmidt, Ian A. Kinloch, Andrew N. Burgess, and Alan H. Windle. The Effect of Aggregation on the Electrical Conductivity of Spin-Coated Polymer/Carbon Nanotube Composite Films. Langmuir 23, 5707-5712 (2007).

[91] Fabian Coupette, Long Zhang, Björn Kuttich, Andrei Chumakov, Stephan V. Roth, Lola González-García, Tobias Kraus and Tanja Schilling. Percolation of rigid fractal carbon black aggregates. J. Chem. Phys. 155, 124902 (2021).

[92] N. Lebovka, L. Bulavin, V. Kovalchuk, I. Melnyk, K. Repnin, Two-step percolation in aggregating systems. Condensed Matter Physics 20, 13602 (2017)

[93] Ruibin Ma, Guangyao Mu, Huan Zhang, Jun Liu, Yangyang Gao, Xiuying Zhao, Liqun Zhang. Percolation analysis of the electrical conductive network in a polymer nanocomposite by nanorod functionalization. RSC Adv. 9, 36324 (2019).